

**Developing an Analytical Model for Charge  
Transport in Organic Solar Cells through  
Simulation of Photocurrent**

by

Xinrui Zhu

Submitted to the Department of Physics  
in partial fulfillment of the requirements for the degree of

Bachelors of Arts

at

Mount Holyoke College

May 2021

©Mount Holyoke College

Author .....  
Department of Physics  
May 11th

Certified by .....  
Katherine E. Aidala  
Professor of Physics  
Thesis Supervisor

Accepted by .....  
Alexi C. Arango  
Chair, Department of Physics



# Developing an Analytical Model for Charge Transport in Organic Solar Cells through Simulation of Photocurrent

by

Xinrui Zhu

Submitted to the Department of Physics  
on May 11th, in partial fulfillment of the  
requirements for the degree of  
Bachelors of Arts

## Abstract

In order to develop next-generation solar cells with higher efficiency, it is important to use charge transport mechanism in a Current-Voltage (IV) model of solar cells. Therefore, we are working on developing an analytical model for current in solar cells in which the charge transport is typically governed by traps. The devices we focus on are planar bilayer organic semiconductor solar cells, and aspects of our model have the possibility of extending to other general devices with bilayer semiconductors, including diodes and transistors.

The analytical model was previously developed based on experimental work, focusing on the dark current of the solar cell. This thesis will present how we use simulation to further validate and improve our analytical model. I will introduce the basic principles of the simulation software, GPVDM, which allows us to simulate current and extract useful parameters of solar cells. Through simulation, we determine methods of correcting for series resistance and extracting the compensation voltage. We then create a new analytical equation for photocurrent, allowing us to fit the photocurrent and extract the compensation voltage. We show that this compensation voltage is proportional to the energy difference at the donor/acceptor interface. While we extended our analytical model to include photocurrent, we also identified a number of open questions and next steps to follow to continue improving and validating the model.

Thesis Supervisor: Katherine E. Aidala  
Title: Professor of Physics



# Acknowledgments

When I first started to write the introduction, it was the March 2020. At that time, the Covid just came. I flew to March meeting and was told it was canceled. The classes were cancelled, and everyone was saying goodbye to each other. I decided to write a thesis on the experimental work I have done on bilayer transistors and waited for the restart of our lab.

In the spring of 2020, our lab were only left with Kathy, Christina, and I. We still held group meeting every week to chat and read journals. I moved out of my double at 1837 and moved into a single room at Mandelle.

In the summer of 2020, I was told that we can work on simulating solar cells. Although I enjoy working in lab, I soon got obsessed with doing simulation. It was a great summer. Everyday, I slept, ate, walked, and did simulation. I experienced loneliness and happiness at the same time, and my work always comforted and accompanied me.

In the fall of 2020, I chose to exploring more open questions in simulation. My original goal was to study the voltage distribution across the solar cells. With some random inspiration, I found out a way to extract compensation voltage from simulation and created a new fit equation for photocurrent.

Now, it is the spring of 2021, and I almost complete this thesis. I cannot complete this thesis without the generous help and support from people around me. I want to say thank you to all of them sincerely.

First of all, I would like to say thank you to Kathy! I cannot use words to describe how important Kathy is for me and how grateful I am for Kathy, because it is infinite. Kathy is the first person who reads my thesis, who has seen all my embarrassing rough draft. Kathy gave me detailed feedback on each word and revised my thesis much more than I did. Whenever I have a question, Kathy is always there to help. We talked about this thesis through Slack, on Zoom, and at the gazebo next to lower lake. When I do not know how to express my ideas clearly, Kathy always understand what I am trying to say and find the most appropriate expression for me. When I was

taking Electronics with Kathy, I sometimes cannot read her handwriting comments, and right now, I am an expert at understanding her hand writing comments. The story between Kathy and I is much more than this thesis. It's even more than the invincible summers and my three years at Mount Holyoke.

Also, I would like to say thank you to Alexi! Alexi is very special for me, and I am always impressive by how creative and brilliant he is, especially looking at the incredible model for current in solar cells proposed by him. Without Alexi, this interesting and amazing project on solar cells will not exist. Moreover, Alexi helped me a lot with the simulation. The development of the photocurrent model is actually most Alexi's work, and what I did is to test the models. When I share any ideas with Alexi, Alexi can always turn it into reality, such as the photocurrent function. Also, when I ask Alexi questions, he is always very patient in offering detailed explanations for the physics and useful plots.

I am so happy to work with both Kathy and Alexi. In addition, I met many supportive people in our lab. I would like to say thank you to Christina, Ayla, and Ji-Won for spending the Summer of 2020 together in starting GPVDM. I also would like to say thank you to all the other members in our lab, including the alumnae and new students, Hadley, Janice, Ye, Ashley, Maryann, Gillian, Sue, Olivia, Charlotte, Kareena, and Claudia. As the Covid comes, I seems to lose the ability of telling difference between time. Today feels like the same as the first day that I enter the lab, for the excitements.

I would like to say thank you to my cohorts—Yuqi Zhang, Yi An, Jingyi Dai, Wenjun Liu, Ningjing Ma, and Jingyi Wu. Especially thanks to Jingyi Dai, my roommate at 1837, who also borrowed me her large screen laptop in the summer of 2020. They make my life at Mount Holyoke unique.

I would like to say thank you to my family. My mom and my dad encourage all the dreams I have. Actually, I would like to say I love you!

I also would like to say thank you everyone at Physics Department, Astronomy Department, and all the other departments at Mount Holyoke College.

Thank you to my thesis committee, Kathy, Alexi, and Professor Wei Chen! Thank

you to my advisor Mark Peterson, who is so interesting and knowledgeable. Thank you to Neal, Spencer, Kerstin, Nicole, Jason, Eileen, Darby, Tom, Gary, David, Lori, Benfey, and Sam...

I also would like to say thank you to more people. The gratitude is an endless list. Everyone I have met is so amazing! If I need to summarize in one sentence, I would like to say thank you to the world, and thank you, Universe!

Einstein has said, “There are two ways to live your life. One is as though nothing is a miracle. The other is as though everything is a miracle.” I am the later case :) There are many unexpected things that come naturally and work well, just like how I write out this thesis. I probably should say thank you to myself for trusting myself, keeping dreaming, working hard, and going with the flow.

Last but not least, thank you to whoever is reading this thesis—your observation makes my work meaningful! Thank you so much! Have a nice day!



# Contents

<b>1</b>	<b>Introduction</b>	<b>19</b>
1.1	Introduction to Solar Cells . . . . .	19
1.1.1	Future Energy for Civilization . . . . .	19
1.1.2	History of Using Solar Energy . . . . .	20
1.2	Physics of Solar Cells . . . . .	21
1.2.1	Energy Bands in Semiconductors . . . . .	21
1.2.2	Basic Structures of Solar Cells . . . . .	26
1.2.3	Current and Efficiency of Solar Cells . . . . .	27
1.2.4	Compensation Voltage . . . . .	32
1.2.5	Traps along Energy Bands . . . . .	33
1.2.6	Charge Recombination . . . . .	35
1.3	An Analytical Models for Current in Solar Cells . . . . .	37
1.3.1	Prevalent Solar Cells Models . . . . .	37
1.3.2	Our Analytical Model for Current in Solar Cells . . . . .	39
1.3.3	Voltage Dependent Charge Transport Mechanisms . . . . .	40
1.3.4	Circuit Diagram and Mathematical Formula . . . . .	46
<b>2</b>	<b>Techniques</b>	<b>53</b>
2.1	Solar Cells in GPVDM simulation . . . . .	53
2.2	Basic Settings and Default Simulation . . . . .	56
2.3	Output in GPVDM . . . . .	61
2.3.1	Dark JV curve and Light JV curve . . . . .	61
2.3.2	Finding the True Compensation Voltage . . . . .	61

2.3.3	Other characteristics that could be extracted from GPVDM . . . . .	66
2.4	Fitting the Simulation in Datagraph . . . . .	66
<b>3</b>	<b>Photocurrent</b>	<b>71</b>
3.1	Original Equation for Photocurrent . . . . .	71
3.2	Correcting Voltage for Series Resistance . . . . .	73
3.3	Adding Power Laws in the Photocurrent . . . . .	76
3.4	Compensation Voltages Extracted from the New Fit Equation and the Interfacial Energy Difference . . . . .	79
<b>4</b>	<b>Discussion and Open Questions</b>	<b>85</b>
4.1	Extracted Compensation Voltages Depend on Trap Parameters . . . . .	85
4.2	Development of Dark Current Model . . . . .	90
4.3	Unifying Powers in both Photocurrent and Dark Current . . . . .	93
4.4	Assess the analytical model with experimental data . . . . .	95
4.5	Summary and Future Plans . . . . .	97
<b>A</b>	<b>Realistic Electric Parameters</b>	<b>101</b>
<b>B</b>	<b>Full Dark Current Equation</b>	<b>105</b>

# List of Figures

1-1	Energy Bands of Metals, Semiconductors and Insulators [1] . . . . .	22
1-2	Schematic band diagram, density of states, Fermi-Dirac distribution, and the carrier concentrations for (a) intrinsic, (b) n-type, and (c) p-type semiconductors at thermal equilibrium [2] . . . . .	23
1-3	Band Bending at the Interface of Donor and Acceptor . . . . .	26
1-4	A Typical Solar Cell with SubPC as the Donor Layer . . . . .	26
1-5	A Typical JV Curve of Dark Current in Linear-Linear Scale . . . . .	28
1-6	A Typical JV Curve of Dark Current in Log-Log Scale . . . . .	29
1-7	A Typical JV Curve of Light Current . . . . .	30
1-8	A Typical IV Curve of Photocurrent . . . . .	31
1-9	Electrons encounter traps as they move along the LUMO band . . . . .	33
1-10	The Exponential Distribution of Traps. Green curve and blue curve are two different distributions of traps. The horizontal segments represent the characteristic trap depth (also known as “tail slope” in GPVDM) of each distribution. The x axis represents the trap density of states, and the y axis represents conduction band/LUMO. When the y axis is zero, we are the energy level of the band (LUMO). Trap states have lower energy than the LUMO. [3] . . . . .	34
1-11	IV Characteristics for a Diode . . . . .	38
1-12	An equivalent circuit of the one-diode model in a solar cell [4] . . . . .	38
1-13	I-V characteristic curve in double-logarithm scale [5] . . . . .	39
1-14	The defined positive direction for electrons and holes in dark current . . . . .	40
1-15	A Band Diagram below Injection . . . . .	41

1-16	A Band Diagram around Injection . . . . .	42
1-17	A Band Diagram above Injection . . . . .	43
1-18	A Band Diagram for photocurrent below Injection . . . . .	45
1-19	A Band Diagram for photocurrent around Injection . . . . .	46
1-20	A Band Diagram for photocurrent above Injection . . . . .	47
1-21	The Physics of Different Contributions . . . . .	48
1-22	Circuit Diagram for Charge Transport Mechanisms in Dark Current . . . . .	49
1-23	A Typical Fit for Dark Current using our Analytical Model . . . . .	51
2-1	The Structure of Layers in Solar Cells. . . . .	56
2-2	The Energy Level for Donor, Middle, and Acceptor Layers in a Default Simulation. . . . .	57
2-3	The electrical parameters for the donor layer in a default simulation. . . . .	58
2-4	The electrical parameters for the middle layer in a default simulation. . . . .	58
2-5	The electric parameters for the acceptor layer in a default simulation. . . . .	59
2-6	The Shunt Resistance and Series Resistance of a default simulation . . . . .	59
2-7	The settings of electrodes in a default simulation . . . . .	60
2-8	Electrical Mesh Points in a default simulation . . . . .	60
2-9	The band diagram in GPVDM at 0 applied voltage. $E_v$ , $E_c$ are valence band and conduction bands. $F_n$ , $F_p$ are quasi Fermi levels. The general slopes of the valence band and conduction band are negative. . . . .	62
2-10	The band diagram in GPVDM at 1.24 applied voltage. The valence band and conduction band are roughly flat. . . . .	62
2-11	The band diagram in GPVDM at 3V applied voltage. The general slopes of the valence band and conduction band are positive. . . . .	63
2-12	The conduction bands and valence bands for device at 0V, 1.24V, and 3V applied voltages in GPVDM. . . . .	63
2-13	The plot of potential from GPVDM at different applied voltages. . . . .	64

2-14	Potential plot at the compensation voltage, where the left point is equal to the middle point is equal to the right point as shown by the dashed line of 1.285 eV. . . . .	65
2-15	Fitting panel in Datagraph, setting the initial value for f as 10 . . . . .	67
2-16	Fitting panel in Datagraph, setting the initial value for f as 20. Note the fit fails because f cannot be negative. . . . .	67
2-17	Fitting panel in Datagraph, setting the initial value for f as 7.44 . . . . .	68
2-18	A bad fit of photocurrent. The fit range is from -0.2V to 0.725V. . . . .	68
2-19	A good fit of photocurrent. The fit range is from -0.2V to 0.837V. . . . .	69
3-1	A typical original photocurrent fit with parameters a, b, c, and f . . . . .	73
3-2	Before and after correcting for series resistance for dark current, light current and photocurrent: dashed lines represent current before correcting for series resistance and solid lines represent current after correcting for series resistance . . . . .	75
3-3	The old photocurrent fit for device with and without traps. . . . .	77
3-4	A typical new photocurrent fit with power laws . . . . .	78
3-5	The photocurrent of three devices with 0.1 light intensity, 1 light intensity, and 10 light intensity. The corresponding compensation voltages extracted from the photocurrent fit are 1.20V, 1.21V, 1.21V . . . . .	80
3-6	The plot of compensation voltages from photocurrent fit versus the compensation voltages from GPVDM. we fit a line with slope of one to the data, and got the fit equation as $-0.01+x$ . The little offset is acceptable compared to the compensaion voltages around 1.2V. The root mean square of the fit is -0.0119, which is also very small. . . . .	81
3-7	The photocurrent data and fit for three devices with energy difference 1.3 eV, 1.4 eV, and 1.5eV. The corresponding compensation voltages are 1.07V, 1.17V, and 1.27V. . . . .	82

3-8	The relationship between compensation voltage and energy difference. The dashed line is fitted by software Datagraph with the function $y = 0.21024 + 1.0164x$ . The root mean square is 0.0018443. . . . .	83
4-1	The plot of compensation voltages extracted from GPVDM versus compensation voltages extracted from photocurrent. Points A, B, C are devices with the same trap parameters: trap density $5.4e24$ and trap depth 0.15 eV. Points D, E, F, G are devices with different trap parameters. Device D has trap density $1e24$ and trap depth 0.15 eV; Device E has trap density $1e25$ and trap depth 0.15 eV; Device F has trap density $5.4e24$ and trap depth 0.13 eV; Device G has trap density $5.4e24$ and trap depth 0.17 eV. The dark blue line is fitted to points A, B, C with fit equation $y = 0.00082346 + x$ . For the fit, the slope is set to be one, and the root mean square is 0.0021. . . . .	86
4-2	The relationship between the compensation voltage extracted from the photocurrent and the interfacial energy difference no longer holds when we change the trap parameters of the device. The dark blue line is fitted to points A, B, C with fit equation $y = (-0.22918) + x$ . For the fit, the slope is set to be one, and the root mean square is 0.0021651. . . . .	87
4-3	The relationship between the compensation voltage extracted from the GPVDM and the interfacial energy difference no longer holds when we change the trap parameters of the device. The dark blue line is fitted to points A, B, C with fit equation $y = (-0.23) + x$ . For the fit, the slope is set to be one, and the root mean square is 0. . . . .	88
4-4	Typical positions of compensation voltages in dark current fit. The compensation voltages are marked by the black + signs. Note that they are located where the pink (recombination) and green (transport) lines intersect. . . . .	91

4-5	The plot of the difference in quasi Fermi levels at the interface versus the effective voltage. The quasi Fermi levels difference is calculated by the electron quasi Fermi level minus the hole quasi Fermi level as determined by GPVDM. The black + sign marks the position of the compensation voltage. . . . .	92
4-6	The plot of M from dark current fit versus F from the photocurrent fit. Both M and F represent the fitting parameters of the recombination term of the solar cells. . . . .	94



# List of Tables

3.1	A typical example of correcting for the series resistance . . . . .	75
3.2	The extracted compensation voltages from GPVDM and photocurrent for devices with difference energy difference at the interface. . . . .	80
4.1	The table of energy difference, compensation voltage from photocurrent and simulation, and the fitting parameters for recombination term in dark current (M) and photocurrent (F). . . . .	94
4.2	Fitting the same experimental data with series resistance equal to 10 $\Omega$ , 50 $\Omega$ , and 100 $\Omega$ . . . . .	96
A.1	The comparison between the simulation electric parameters that I use and the more realistic parameters our group recently found. Donor Layer 1 shows the parameters I use in the simulation for an ideal symmetrical device. Donor Layer 2 is based on matching the simulation data with the experimental data, which provides more realistic parameters. . . . .	101
A.2	The comparison between the simulation electric parameters that I use and the more realistic parameters in acceptor layer. . . . .	102
A.3	The comparison between the simulation electric parameters that I use and the more realistic parameters in middle layer. . . . .	103



# Chapter 1

## Introduction

### 1.1 Introduction to Solar Cells

#### 1.1.1 Future Energy for Civilization

With the development of technology, the material life on the Earth is prosperous, but the rapid growth generates severe problems, including the loss of sustainability. People take the use of energy for granted, while they are blind to the fact the non-renewable energy will be depleted in the foreseeable future. For the continuation of our civilization, it is urgent to replace non-renewable energy with renewable energy.

Among many kinds of renewable energy, solar cells are one of the most accepted. The commercial solar cells made of silicon have already produced renewable energy for countries all over the world. In comparison, the next-generation solar cells made of disordered materials are cheaper and more flexible, which could be applied to a broader range of uses and finally become the future energy for human beings.

In this Thesis, I will present our research on the fundamental principles of next-generation solar cells. Before diving into the interesting physics, let's first go through a brief history of solar energy on Earth.

### 1.1.2 History of Using Solar Energy

We live in the Solar System, where the Sun nurtures all the planets, especially the Earth. Sunlight not only creates day and night, but also participates in many chemical reactions, such as the photosynthesis effect for plants. In addition, people began to use solar power directly since ancient times, by basking themselves on sunny days. There are also people who made fires by passing sunlight through convex lenses.

The revolution of solar energy came in 1839, when Becquerel first discovered the photovoltaic effect. He observed that an electric circuit produced more current when he illuminated the electrodes [6], which indicated that solar energy could be transferred directly into electricity. With the collaboration of many chemists and physicists, Fritts created the first working selenium solar cell in 1883 [7]. In 1905, Einstein published a paper about the photoelectric effect and explained how light carries energy [8]. The developments in physics theory helped people understand more about the phenomenon and stimulated the public's interest in solar cells.

In 1954, Bell lab created a more practical solar cell with silicon. Silicon solar panels were used to power spacecraft from the 1950s to 1960s. In the 1970s, the oil shortage brought the public's attention to solar cells again. President Jimmy Carter installed solar panels in the White House. As technology improves, solar panels average between 15 and 23 percent efficiency and can cost as low as 0.5 dollars per watt currently. Many individuals, communities, companies, and countries begin to use solar cells to replace fuel energy. Mount Holyoke College is still in the process of doing that. Serving as a role model, physics professor Arango at Mount Holyoke College has already built and lived in a sustainable house powered by solar cells.

As solar cells' share in the energy market keeps increasing, the next generation solar cells are made of multi-layer novel materials such as organic semiconductors, aiming at low costs and high efficiency for the cells.

The improvement of solar cells' efficiency is always the key question. Most groups try hard in fabricating more efficient solar cells by studying the device parameters. In contrast, our group is interested in understanding the fundamental physics of charge

transport inside the organic solar cells and creating an analytical model for current in solar cells, which could lead to the next revolution in the field of solar cells.

## 1.2 Physics of Solar Cells

In order to understand the behavior of solar cells, we need to learn about the related physics. This section will introduce energy bands, basic structures, current, efficiency, compensation voltage, traps, and charge recombination in solar cells.

### 1.2.1 Energy Bands in Semiconductors

The Pauli Exclusion Principle states that no two electrons can exist in the same state (same spin and energy level), so atomic orbitals split and have discrete energy [2]. When multiple energy levels sit next to each other, energy bands are created.

In a material, the outermost band with occupied electrons is the valence band, which is also known as the Highest Occupied Molecular Orbital (HOMO). The conduction band is the next highest band in energy, which is called the Lowest Unoccupied Molecular Orbital (LUMO). Most electrons are in the valence band, but some electrons are able to be excited from the valence band into the conduction band, and move freely there to form a current (movement of charge). When an electron leaves the valence band, the absence of the electron will leave a positive charge called a hole in the valence band.

The band gap is the energy level difference between the valence band and conduction band. The energy level in the band gap are levels that do not exist. They are sometimes called forbidden levels. If the electrons in the valence band have enough energy, they can overcome the band gap to enter the conduction band. Energy bands show where the electrons are possible to exist. In contrast, the band gap indicates the region where electrons are impossible to exist. Energy bands can be used to suggest the conductivity of a material, as shown in Figure 1.1. For metal (conductors), the valence band and conduction band overlap, so that electrons can easily move—or conduct—in metal. For an insulator, the band gap is large enough to make the elec-

trons impossible to be excited into a conduction band. For semiconductors, the band gap is smaller than that of an insulator while larger than that of a conductor, which creates conductivity depending on the external conditions (pressure, temperature).

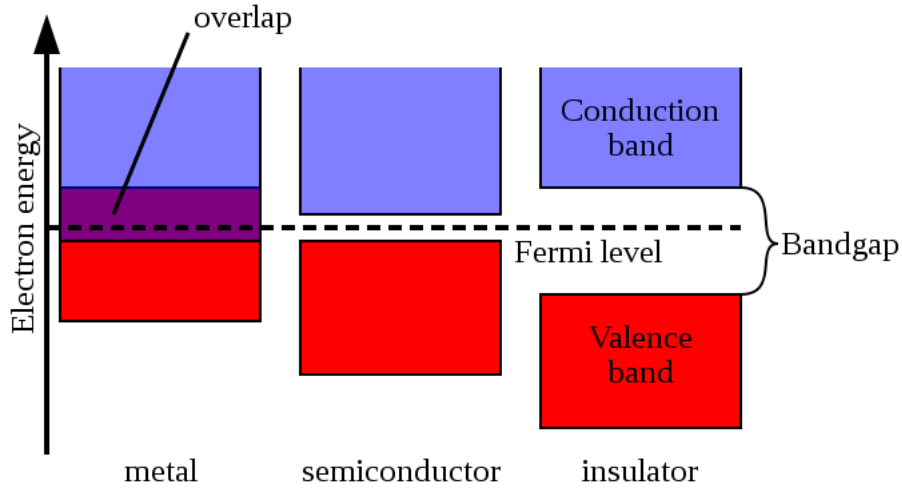


Figure 1-1: Energy Bands of Metals, Semiconductors and Insulators [1]

There is a specific energy called the Fermi level, named after Enrico Fermi, the scientist who first proposed it. The Fermi level indicates the maximum electron energy at absolute zero temperature. We could use Fermi Dirac statistics to determine the charge distribution at a specific temperature with the equation below.

$$f(E) = \frac{1}{1 + e^{\frac{E-E_f}{kT}}} \quad (1.1)$$

Equation 1.1 is the Fermi function or Fermi Dirac distribution, where  $f(E)$  is the probability of finding an energy level  $E$  to be occupied by an electron,  $E_f$  is the Fermi level energy,  $k$  is the Boltzmann constant, and  $T$  is the temperature. The equation suggests that the probability of finding an electron at the Fermi level energy is  $\frac{1}{2}$ .

The density of states ( $N$ ) describes the number of available energy states of charge carriers at a certain energy level per unit volume [9]. The integral of the density of states over a range of energy is called the effective density of states in the conduction band ( $N_c$ ) and valence ( $N_v$ ) band. In other words,  $N_c$  and  $N_v$  represent all the distributed electron states in the conduction band and hole states in the valence

band. Equation 1.2 and Equation 1.3 show the detailed integral.

$$N_c = \int_{E_c}^{\infty} N(E)dE \quad (1.2)$$

$$N_v = \int_{-\infty}^{E_v} N(E)dE \quad (1.3)$$

The unit of density of states is per volume per energy, and the unit of effective density of states is per volume [2].

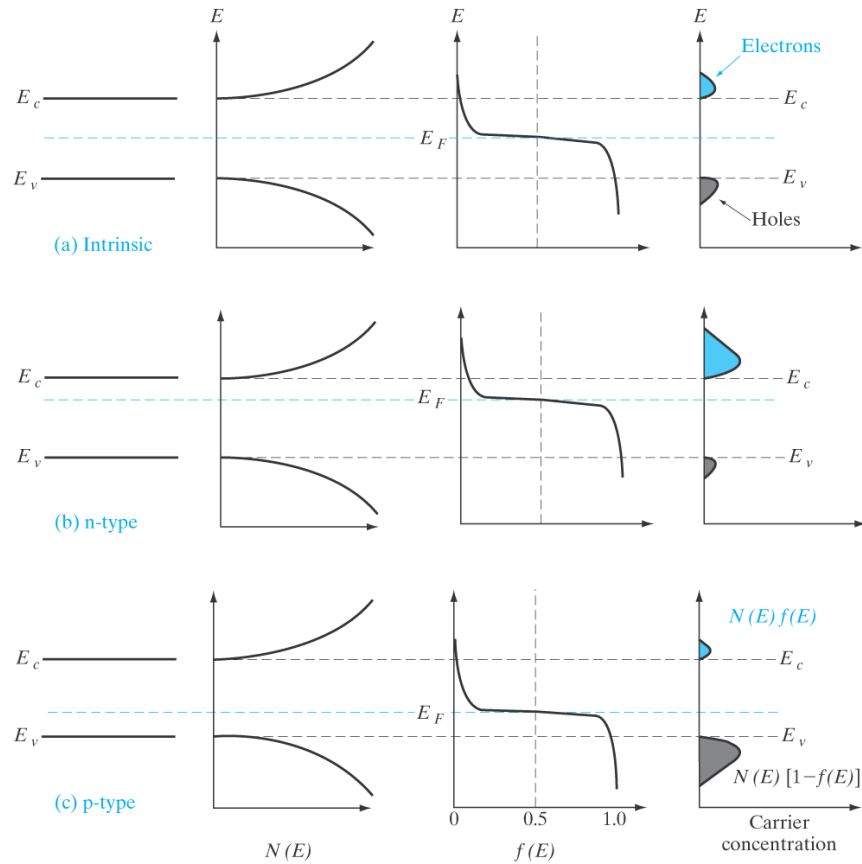


Figure 1-2: Schematic band diagram, density of states, Fermi-Dirac distribution, and the carrier concentrations for (a) intrinsic, (b) n-type, and (c) p-type semiconductors at thermal equilibrium [2]

The multiplication of effective density of states and Fermi Dirac Distribution at the corresponding energy is the concentration of charges, because multiplying the

possible states with the probability gives us the occupied states—concentration of carriers. Figure 1-2 shows the different positions of Fermi level result in a different distribution of electrons and holes. It is reasonable that n-type material has a larger electron concentration, and similar trends could be found in the intrinsic (neither n-type nor p-type) material and the p-type material.

In the situation where the absolute value of  $E - E_f$  is larger than  $kT$ , the Fermi distribution from Equation 1.1 could be simplified into:

$$f(E) = \frac{1}{1 + e^{\frac{E-E_f}{kT}}} \approx e^{\frac{-(E_f-E)}{kT}} \quad (1.4)$$

Thus, we can calculate the thermal equilibrium electron and hole concentration ( $n$  and  $p$ ) from the effective density of states and Fermi level as shown below:

$$n = N_c f(E_c) = N_c e^{\frac{-E_c+E_f}{kT}} \quad (1.5)$$

$$p = N_v [1 - f(E_v)] = N_v e^{\frac{E_v-E_f}{kT}} \quad (1.6)$$

$f(E_c)$  is the probability of finding an electron at the conduction band. Similarly  $f(E_v)$  is the probability of finding an electron at the valence band. However, we want to know the hole distribution. So, the probability of finding an empty state (not occupied by electron, aka hole) in the valence band is  $[1 - f(E_v)]$ .

There is a comparable term with Fermi Level called quasi Fermi Level, which describes the equivalent effect of Fermi Level under the non-equilibrium conditions, such as when the device is in use and there are injected electrons and holes. For the quasi Fermi level, we need to think about electrons and holes separately, because the quasi Fermi Level of electrons is not necessarily equal to that of holes. An analogy is that Fermi Level is splitting into electron quasi Fermi Levels and hole quasi Fermi Levels. The position of quasi Fermi Levels depends on the hole and electron concentrations, as given in the equations below:

$$E_{fn} = E_c - kT \ln\left[\frac{N_c}{n}\right] \quad (1.7)$$

$$E_{fp} = E_v - kT \ln\left[\frac{N_v}{p}\right] \quad (1.8)$$

where  $E_{fn}$  and  $E_{fp}$  are the quasi Fermi levels for electrons and holes,  $E_c$  and  $E_v$  are the energy levels for conduction band and valence band,  $N_c$  and  $N_v$  are the effective density of states at conduction bands and valence band, and  $n$  and  $p$  are the thermal equilibrium concentration for electrons and holes [10].

The position of Fermi Levels could also reveal whether a semiconductor is n-type or p-type. When the Fermi Level is closer to the valence band, the semiconductor will have more electrons compared to holes, so it is the p-type semiconductor. In p-type material, the majority of carriers are holes. In comparison, when the Fermi Level is closer to the conduction band, this type of semiconductor is n-type and its majority carriers are electrons. We also call p-type materials donor and n-type materials acceptor in a solar cell, because we usually select the p-type materials that have higher LUMO than the n-type material, so electrons tend to move from p-type to n-type materials.

When the p-type and n-type materials are in contact, their different Fermi levels have to align toward each other to form an equilibrium state of the energy at the interface. Meanwhile, the energy bands far away from the interface are not affected and stay constant according to their intrinsic chemical properties. Therefore, band bending will appear at the interface of two materials, also known as a heterostructure. The shape of the band bending could change at different applied voltages, as illustrated in Figure 1-15, Figure 1-16, and Figure 1-17 in the later section. Figure 1-3 is an example of band bending at a positive bias.  $\Delta E$  is the difference between the HOMO of the donor layer and the LUMO of the acceptor layer, which is known as the energy difference between donor and acceptor.

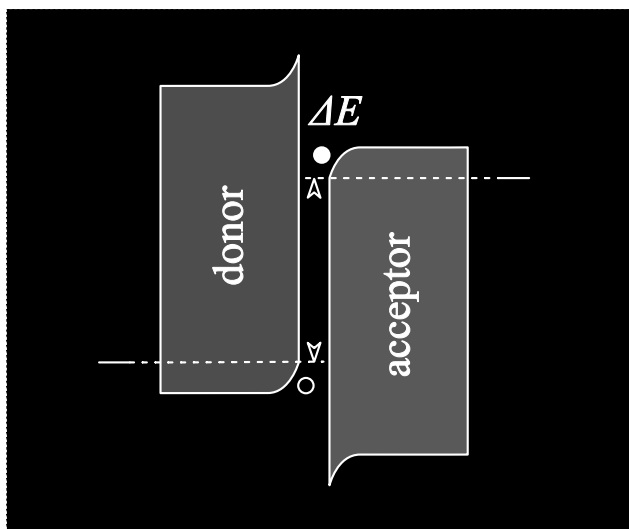


Figure 1-3: Band Bending at the Interface of Donor and Acceptor

### 1.2.2 Basic Structures of Solar Cells

Solar cells are based on the photovoltaic effect—electrons in the valence band will absorb energy from light and be excited to the conduction band where they can form current.



Figure 1-4: A Typical Solar Cell with SubPC as the Donor Layer

One of the next-generation solar cells we study is the bilayer planar organic solar cell. Figure 1-4 shows the schematic of a typical device, in which SubPC is the donor layer and the acceptor layer is in black. The important thing to notice is that donor and acceptor layers are where the photovoltaic effect happens in a bilayer solar cell.

The ITO and Ag layers are electrodes, and the BCP and MoO<sub>3</sub> layers are transparent layers for better performances.

### 1.2.3 Current and Efficiency of Solar Cells

In a solar cell, the current is generated when an external voltage is applied to shift the energy bands. There are three typical types of current that are often used to characterize solar cells: dark current, light current, and photocurrent.

J-V and I-V curves are two kinds of graphs that can describe the dependence of current on voltage. J-V curves are plots of current density (J) versus voltage (V), and I-V curves are the plots of current (I) versus voltage. It is more convenient to use current density in analyzing characteristics in solar cells, because it removes the impact of surface area.

We usually use the J-V curve to analyze solar cells in our research. In later discussion, I may use the expression of current and current density alternatively, and please be aware of their similarities and trivial difference.

#### Dark Current

Dark current is the most fundamental current in solar cells, which is the current due to applied voltage without light. As shown in Figure 1-5 and Figure 1-6, the dark current is very small at low voltages and has a turn-on after a certain voltage. In order to better analyze dark current, we often plot dark current on a log-log scale, in which the slope of each linear segment directly reveals the voltage dependence of current in that section.

This is known as a power law. For example, if the relationship between current and voltage in the linear-linear scale is  $V = ax^A$ , the corresponding relationship on the log-log scale becomes  $\log V = A \log x + \log a$ . Therefore, we could extract the power of x in the linear-linear scale from the slope of  $\log x$  in the log-log form.

Dark current demonstrates the basic movement of electrons and holes under different applied voltage and is the foundation for both light current and photocurrent.

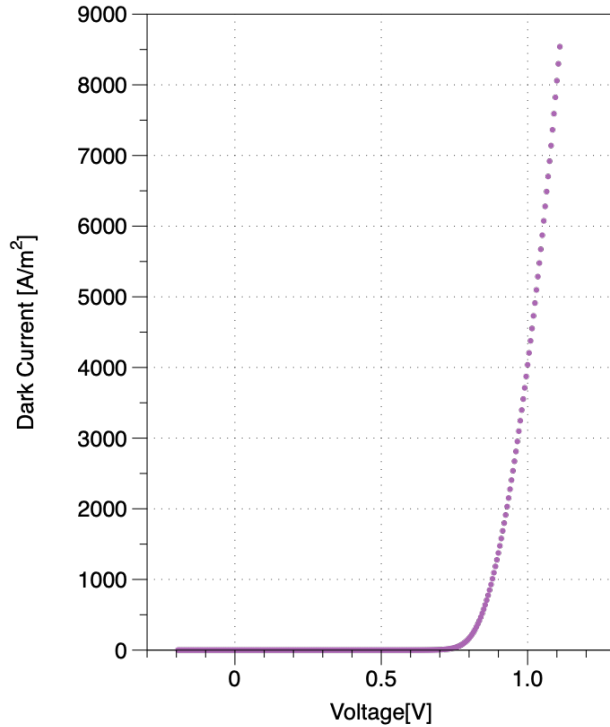


Figure 1-5: A Typical JV Curve of Dark Current in Linear-Linear Scale

More details about the charge transport mechanisms in dark current will be discussed later.

### Light Current

Light current is the current of solar cells under the illumination of light. The photovoltaic effect will excite electrons to the conduction band, leaving holes in the valence band. Thus, there are more charge carriers in the light current compared to the dark current. Another way to understand it is that the current caused purely by the photovoltaic effect is photocurrent, and the light current is the sum of photocurrent and dark current.

As shown in Figure 1-7, the light current is a negative constant at low applied voltages. As the applied voltage increases, the light current goes through a sharp turn-on and becomes positive.

The light current at zero applied voltage is the short circuit current,  $I_{SC}$ . The applied voltage when the light current is zero is the open-circuit voltage,  $V_{OC}$ . These

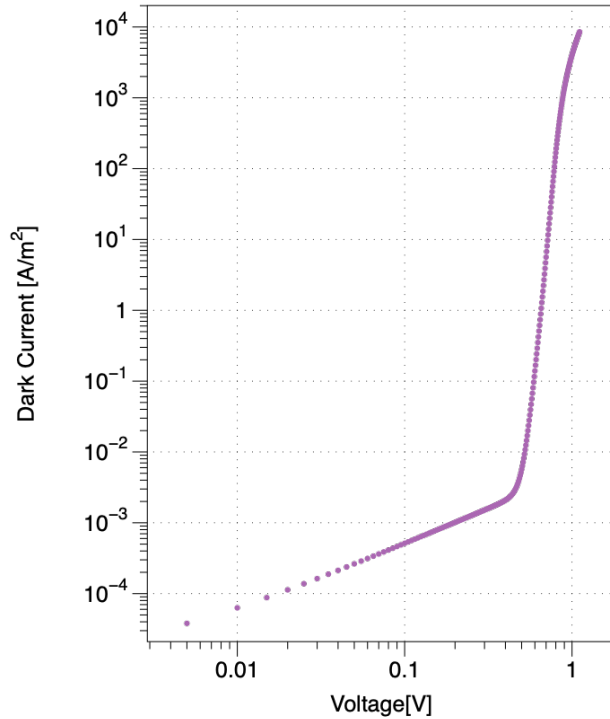


Figure 1-6: A Typical JV Curve of Dark Current in Log-Log Scale

two parameters are often used to estimate the efficiency of a solar cell.

### Efficiency of Solar Cells

When we talk about the efficiency of solar cells, we refer to the maximum efficiency at a point along the light current IV curve.

As introduced above, light current provides short-circuit current,  $I_{SC}$ , and open-circuit voltage,  $V_{OC}$ . Short-circuit current is the maximum current a solar cell could reach, and an open-circuit voltage is a maximum voltage a solar cell could still run effectively. So, the product of  $I_{SC}$  and  $V_{OC}$  is the maximum possible power a solar cell could have. However, the actual maximum power of the solar cell is a point along the light current, where the product of current and voltage is the largest. Because the shape of the light current IV is not a perfect square, the real maximum power of the solar cell is always smaller than the ideal maximum power. The ratio of the real maximum power ( $P_{MP}$ ) and the ideal maximum power of a solar cell are known as the fill factor, FF, where  $P_{MP}$  represents the maximum power in reality:

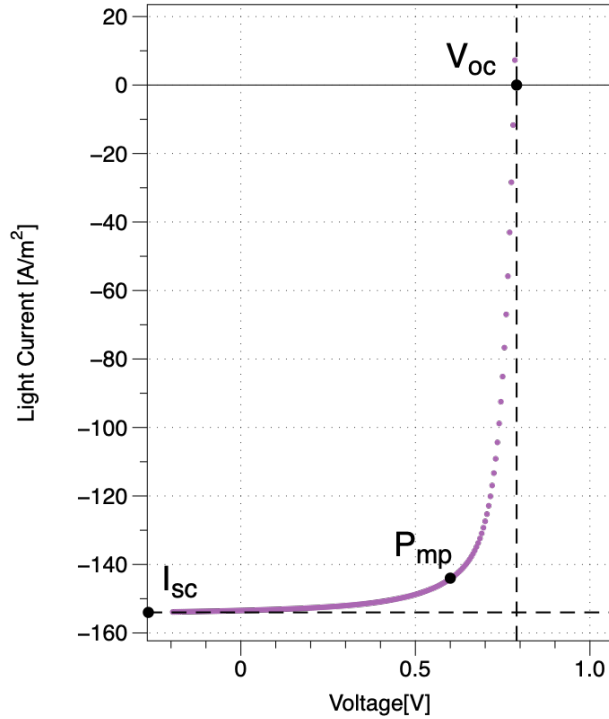


Figure 1-7: A Typical JV Curve of Light Current

$$FF = \frac{P_{realmax}}{P_{idealmax}} = \frac{P_{MP}}{V_{OC} \times I_{SC}} \quad (1.9)$$

The efficiency of a solar cell is defined as the ratio of how much power it produces ( $P_{out}$ ) and how much power we put into it ( $P_{in}$ ). We could calculate the power a solar cell produces by following the equation below:

$$P_{out} = P_{MP} = FF \times V_{OC} \times I_{SC} \quad (1.10)$$

So, the efficiency ( $\eta$ ) of a solar cell is

$$\eta = \frac{P_{out}}{P_{in}} = \frac{FF \times V_{OC} \times I_{SC}}{P_{in}} \quad (1.11)$$

In order to increase the efficiency of a solar cell, we will try to increase the fill factor. The geometric meaning of the fill factor is how square the light current is. We try to make the shape of light current as square as possible. In other words, we would like the turn-on of light current to be as sharp as possible.

## Photocurrent

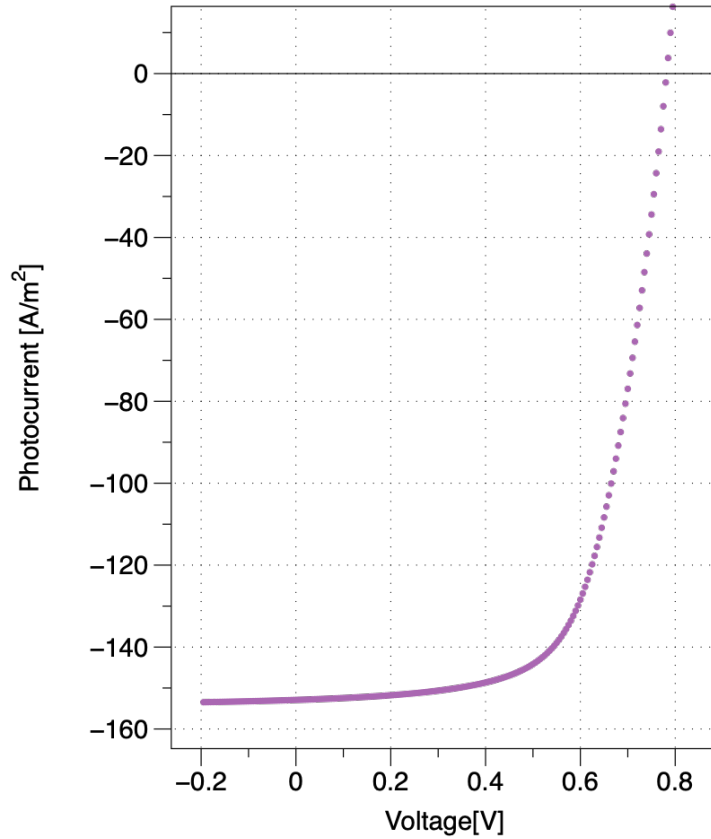


Figure 1-8: A Typical IV Curve of Photocurrent

The photocurrent is the amount of current due to the separation of electrons and holes by the photovoltaic effect, as shown in Figure 1-8. Similar to light current, the photocurrent is a negative constant at low applied voltages. Then, the photocurrent goes through a turn-on, which is usually less sharp than the turn-on of light current. After that, the photocurrent will cross zero and become positive. The mathematical definition of photocurrent is the difference between light current and dark current:

$$I_{photo} = I_{light} - I_{dark} \quad (1.12)$$

For the physical definition, the photovoltaic effect only depends on the light intensities and the intrinsic material properties, so the generation of photocurrent is independent of applied voltage. However, the applied voltage could change how the

photocurrent is collected by the two electrodes and change its direction.

At low applied voltages:

$$|I_{light}| = |I_{photo}| - |I_{dark}| \quad (1.13)$$

At high applied voltages:

$$|I_{light}| = |I_{photo}| + |I_{dark}| \quad (1.14)$$

At low applied voltages, photocurrent is negative and dark current is positive, so the magnitude of the light current is the difference between their absolute values. At high applied voltage, the photocurrent will change its direction and become positive, and the direction of the photocurrent is the same as that of the dark current. Thus, the magnitude of the light current is the sum of the absolute values of photocurrent and dark current. When we consider the Equation 1.12, the negative sign in front of the dark current takes the photocurrent's change of direction into account.

## 1.2.4 Compensation Voltage

In photocurrent, there is a parameter that has a comparable magnitude to the open-circuit of the light current—compensation voltage [11]. However, the compensation voltage is a more reliable way to characterize the photocurrent. By definition, the compensation voltage is where the photocurrent is equal to zero. The open circuit voltage depends on the light intensities, while the compensation voltage does not. The compensation voltage is also independent of the current magnitude and the contacts. Compensation voltage provides useful information about the device. The compensation voltage is related to the recombination at the interface, and we believe that the energy difference between HOMO and LUMO has a one to one relationship with the compensation voltage.

In addition to the compensation voltage, there are other voltage values that researchers use. It is possible for the different voltage terms to be equivalent under

certain conditions. The maximum open-circuit is the open-circuit voltage when the light intensity is infinity. The compensation voltage is believed to be roughly equal to the maximum open-circuit voltage. The flat-band voltage is the voltage when the band diagram is flat. The flat band voltage is equal to the compensation voltage when all the current is drift current.

We use compensation voltage to characterize our device. Pay attention to the fact that the compensation voltage we use in analyzing dark current may not follow the strict definition of the compensation voltage, because it is difficult to measure the photocurrent near zero voltage accurately. It is possible for a photocurrent to never cross zero, especially for real devices. Therefore, we create our algorithm to get the compensation voltage by fitting the photocurrent at relative low applied voltages. Moreover, we assume that most current is drift and use the flat-band voltage from our simulation software to determine the compensation voltage, which allows us to develop our algorithm of extracting compensation voltage from photocurrent.

### 1.2.5 Traps along Energy Bands

Organic materials have many traps, which are electrical defects providing localized states in the band gap between HOMO and LUMO [12].

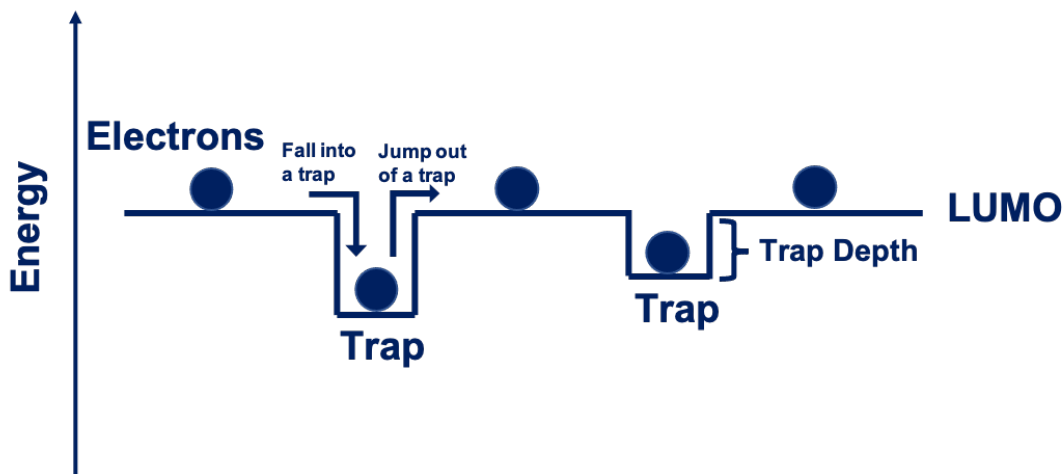


Figure 1-9: Electrons encounter traps as they move along the LUMO band

In a band diagram, electrons naturally move downward to a lower energy level,

and holes naturally move upward to a higher energy level. The energy levels of traps are slightly lower than the conduction band or higher than the valence band. Thus, both electrons and holes are likely to fall into traps when they move along the band.

Figure 1-9 is a schematic diagram for what traps look like along the LUMO and how electrons fall into and jump out of a trap as they move along the energy band. Electrons tend to fall into a trap spontaneously because traps have lower energy. It takes extra energy for an electron to jump out of a trap. The trap depth is the difference between the energy of the band and the trap. The deeper the trap depth, the more difficult it is for an electron to get out, so the electron tends to stay inside the deeper trap for a longer time.

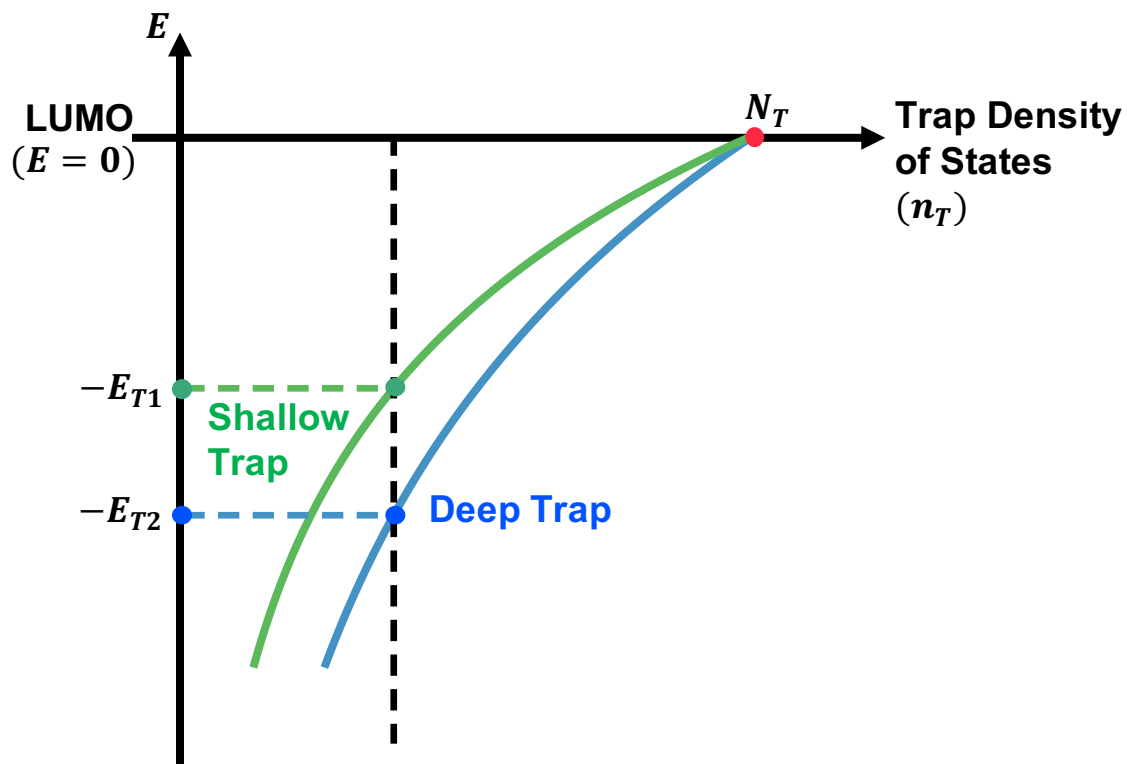


Figure 1-10: The Exponential Distribution of Traps. Green curve and blue curve are two different distributions of traps. The horizontal segments represent the characteristic trap depth (also known as “tail slope” in GPVDM) of each distribution. The x axis represents the trap density of states, and the y axis represents conduction band/LUMO. When the y axis is zero, we are the energy level of the band (LUMO). Trap states have lower energy than the LUMO. [3]

Traps can be divided into two types based on their depths—shallow traps and deep traps. Shallow traps are located closer to the band energy and the deep traps are farther away, as shown in Figure 1-10. For shallow traps, the trap depth is usually less than thermal energy  $k_B T$ , and traps with larger trap depth are deep traps.

As the trap depth increases, the number of traps decreases. Many researchers use a falling exponential or a Gaussian distribution to describe the location of traps in energy near the band edge. No matter which statistical expression is chosen, both distributions aim to reveal the reality that there are more shallow traps than deep traps. For our research, we use the exponential distribution, the simplest way, to describe traps. The exponential decay of trap density in Figure 1-10 is an illustration of our exponential distribution.

Traps can impede the movements of charges by letting charge carriers fall into and jump out of the traps. We include a charge transport mechanism called “Transport” to describe the effect of traps on current. This mechanism is also known as space charge limited current (SPLC) with traps. Below is the common formula that researchers use to describe the SPLC with traps current based on the exponential distribution of traps [12] [13]:

$$J = q^{1-l} \mu_p N_v \left( \frac{2l+1}{l+1} \right)^{l+1} \left( \frac{l\epsilon_S}{(l+1)N_t} \right)^l \frac{V^{l+1}}{d^{2l+1}} \quad (1.15)$$

in which “ $l$ ” is equal to the ratio of the characteristic temperature of the traps and the absolute temperature. The characteristic temperature is proportional to the trap energy. Therefore, what we need to know is that “ $l$ ” depends on the trap energy and is usually larger than 1. The power of voltage in Equation 1.15 is “ $l+1$ ”, which tells us the voltage dependence of space charge limited current with traps is larger than 2 and depends on trap depth.

### 1.2.6 Charge Recombination

Another critical contribution to the current in solar cells is called charge recombination. An electron is a negative charge, and a hole is a positive charge. As a result,

when a hole meets with an electron, they can recombine with each other and become neutral. Thus, we lose an electron and a hole when they recombine. In other words, the charge recombination could decrease the number of charge carriers.

However, electrons are in the conduction band, and holes are in the valence band. Electrons and holes cannot meet unless they change their states. If a charge would like to transition from one state to another, coupling is required. For electronic states, there are two ways of coupling: the electromagnetic spectrum (photons) or the lattice (phonons). For the first case, an electron in the excited state cannot move to a lower state unless there happen to be a photon at the location to remove exactly the energy difference between the two states. This type of recombination is known as radiative recombination. Alternatively, the electron can impart its energy to the lattice and wait for lattice vibrations of the correct energy difference, which can take a long time because the energy of lattice vibrations is typically small, like 0.01-0.1 eV. This process is more likely to happen in trap states at multiple energy levels. An electron can release a small amount of energy to the lattice, then jump into a slightly lower trap state. The electron might move down in energy and the hole might move up in energy. When they get close to 0.5 eV separation, the recombination between holes and electrons is possible to occur spontaneously because of the surrounding thermal energy. This type of recombination is known as non-radiative trap assisted recombination, which is also called Shockley-Read-Hall recombination [14].

The charge recombination that we are most interested in is the radiative recombination at the interface between the donor and acceptor layers, as illustrated in Figure 1-3, which is fundamental for solar cells. Around compensation voltage, both electrons in the acceptor and holes in the donor travel to the interface, where they encounter an energy barrier. There are a large number of electrons and holes buildup at the interface. Moreover, the applied voltage here provides enough energy for the photons to start the radiative recombination. Therefore, massive electrons and holes can meet and recombine very easily across the band gap. We hypothesize that the recombination at the interface explains the rapid turn-on of current in solar cells.

## 1.3 An Analytical Models for Current in Solar Cells

### 1.3.1 Prevalent Solar Cells Models

There are many models for current in solar cells proposed by researchers. However, the most prevalent model is still incomplete today.

Most researchers simply use the Shockley diode model developed for crystalline p-n junctions to describe the behavior of current in organic solar cells. A diode is an electrical device that allows current to flow only in one direction, and Figure 1-11 shows its IV characteristics. The Shockley diode equation describes the exponential dependence in voltage for the forward current in p-n junctions, as shown in Equation 1.16.

$$I = I_S(e^{\frac{qV}{nkT}} - 1) \quad (1.16)$$

where the I is the forward current,  $I_S$  is the saturation current, q represents the charge constant, T is the temperature, k is the Boltzmann constant, and n is the ideality factor. The ideality factor “n” is used to explain variation in current, attributed to traps and other parameters of the device. For example, both references [15] and [16] suggest that the ideality factor is related to charge recombination.

One of the most used solar cell models is the one-diode model, which is also known as the five-parameter model [4]. Paper [17] offers a wide range of literature on different methods to extract parameters for the one-diode model.

In addition to the Shockley diode, the one-diode model includes photocurrent ( $I_{ph}$ ), shunt resistance ( $R_{sh}$ ), and series resistance ( $R_s$ ). Both the shunt and series model the power losses. Figure 1-12 demonstrates how the five parameters add together in an equivalent circuit. The full equation for the one diode model follows:

$$I = I_{ph} - I_S(e^{\frac{qV}{nkT}} - 1) - \left(\frac{V + R_s I}{R_{sh}}\right) \quad (1.17)$$

Some researchers improve the one-diode model by adding more diodes to the model, which forms the two-diodes model and three-diodes model [18] [19]. The main

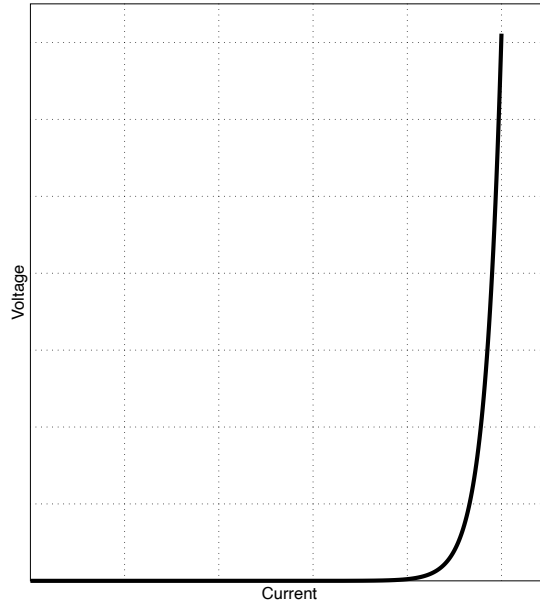


Figure 1-11: IV Characteristics for a Diode

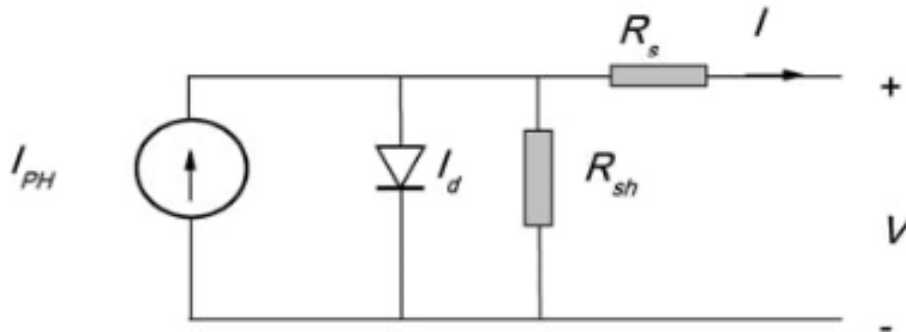


Figure 1-12: An equivalent circuit of the one-diode model in a solar cell [4]

takeaway from those models is still about using the exponential relationship from the Shockley equation to model the behavior of dark current in solar cells. While models may vary on the number of diodes, none of them considers the physics of the organic semiconductors.

Other researchers use computational methods to fit the IV curves [20], [21]. However, one significant drawback for the computational-oriented models is the lack of physical intuition.

A few groups have derived more complicated expressions that include space charge

limited current (SPLC) with traps. However, these analytical expressions usually use piecewise fittings, which lose some information of the system [22][5]. For example, Chaudary et al. analyzed the dark current of a perovskite solar cell by breaking it into four different voltage regimes and performing piecewise fits. They attributed the steepest part of the curve to a regime that behaves as SPLC with traps, which obeys a power law, as shown in Figure 1-13.

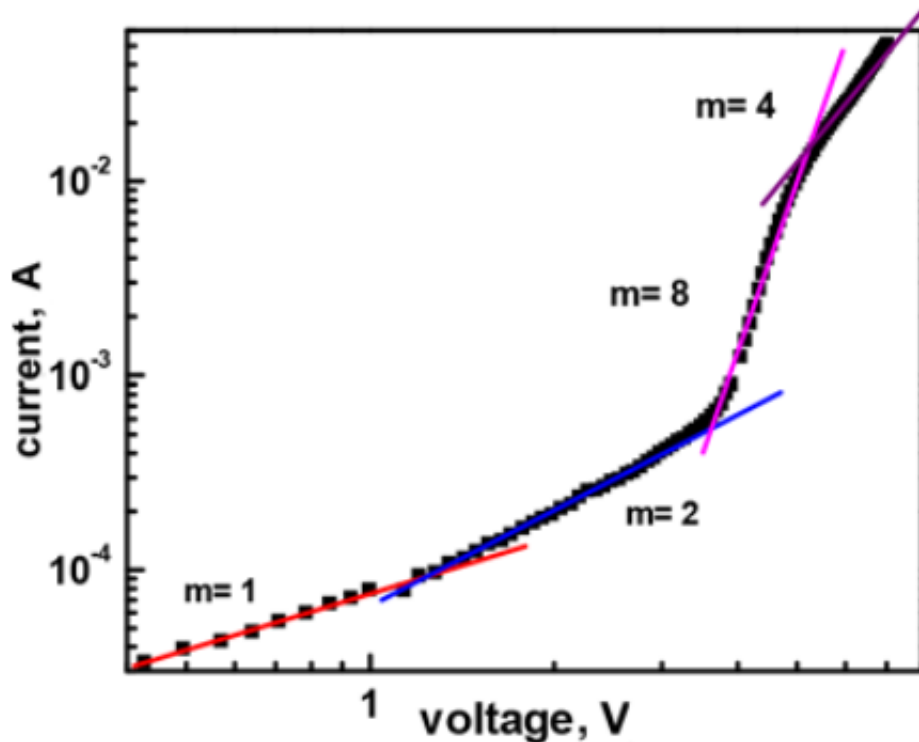


Figure 1-13: I-V characteristic curve in double-logarithm scale [5]

### 1.3.2 Our Analytical Model for Current in Solar Cells

The Aidala Lab and Arango Lab are also developing an analytical model for current in solar cells, which was first proposed by Professor Alexi Arango. Compared to the aforementioned models (one-diode, computational, piecewise fit, etc.), our analytical model provides a thorough explanation for the charge transport mechanism incorporating fundamental physics. We strive to include the relevant physics (recombination, SPLC with traps) as well as a comprehensive consideration of all possible pathways

for the current, including non-idealities like shunt resistance, as will be explained later. Additionally, we extract more reliable characteristic parameters from a continuous fitting along the IV curve. Moreover, we correct for series resistance in our model, which is proved to be important in the analysis of photocurrent [23] [24].

### 1.3.3 Voltage Dependent Charge Transport Mechanisms

Although a solar cell could apply voltage to itself under illumination, We need to apply external voltage to make a solar cell work in dark. We also need the applied voltages to study solar cell's behavior. Applied voltages change the shapes of energy bands, determine the number of charges that could be injected into the bands, and lead to different dominant charge transport mechanisms with different voltage dependencies in the device.

#### Voltage Dependence of Dark Current

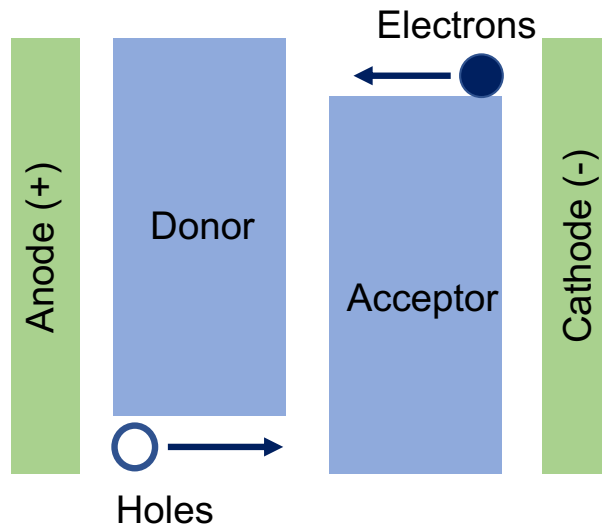


Figure 1-14: The defined positive direction for electrons and holes in dark current

Let's first analyze the behavior of dark current. Remember that the electrode next to the donor layer is the anode (positive) and the electrode next to the acceptor layer is the cathode (negative). Electrons are supplied by the cathode and try to get

into the anode, and vice versa for holes. Positive current is defined as electrons that move from cathode to anode, and holes are opposite. Figure 1-14 helps us review that.

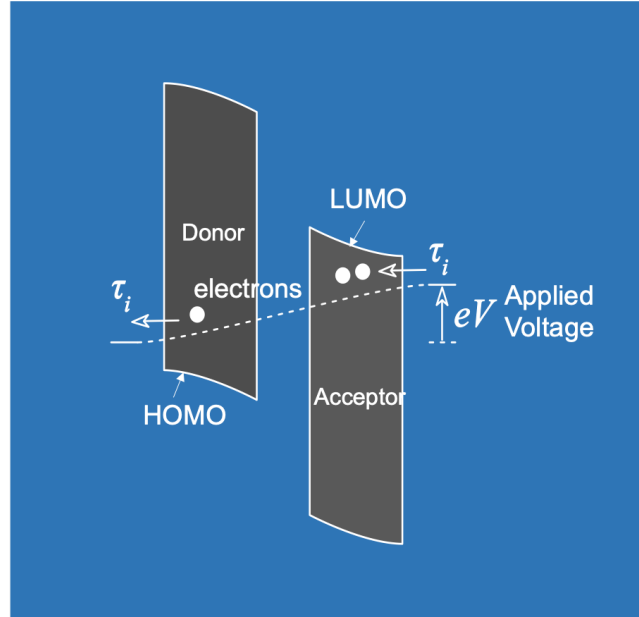


Figure 1-15: A Band Diagram below Injection

When the applied voltage is negative or very small, the band’s general slope is negative, as shown in Figure 1-15. In this situation, the charges are not injected into the bands, because electrons tend to move downward in the band diagrams, and vice versa for holes. There could be a few conduction paths through the device’s defects or filaments of one organic material spanning the electrodes that charges could move along. We call this region the Ohmic Region, where the current is small and directly proportional to voltage. People also call this effect “shunt” resistance [25].

As the applied voltage increases, some electrons and holes could move toward the interface through defects slowly and recombine. We call this region Shunting Region. Notice that the recombination here is at low energy states (the energy difference between electrons and holes is small compared to bandgap), which is also known as non-radiative recombination. This means the current produced by recombination is not prominent. The voltage dependence of the non-radiative recombination is comparable with the voltage dependence of the space charge limited current with traps

when charges move from electrodes to the interface slowly. Therefore, the voltage dependence of the Shunting Region is the mixture of the non-radiative recombination and space charge limited current with traps.

For the Ohmic Region and the Shunting Region, charge carriers are both not injected into bands and are bypassing the standard recombination mechanism at the interface. While both can be considered a “shunt” across the interface at low current, we distinguish these two mechanisms by their voltage dependence.

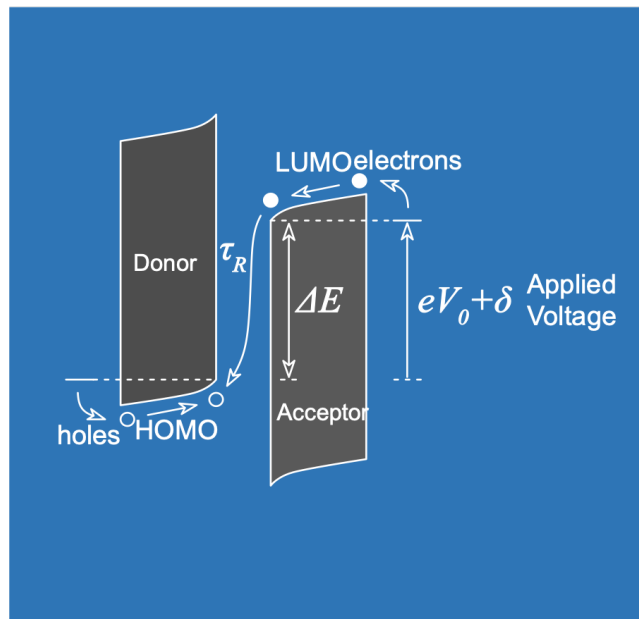


Figure 1-16: A Band Diagram around Injection

When the applied voltage increases to around the compensation voltage, the slope of the bands becomes roughly flat. At this point, it is possible to inject holes and electrons from the electrodes into the HOMO and LUMO bands directly, as Figure 1-16 shows. Along the energy bands, electrons and holes travel to the interface quickly, meet each other, and recombine across the bandgap. Notice the recombination here happens at a high energy state (the energy difference between HOMO of donor and LUMO of acceptor), which has a high voltage dependence that is significantly different from all the other charge transport mechanisms. This is our standard recombination mechanism.

With the massive recombination at the interface, the current in the device will

increase rapidly, and we call this regime the Recombination Region. Experimentally, we observe the Recombination Region obeys a power law. We believe the voltage dependence of the Recombination Region is proportional to the energy difference at the interface, which determines the rate of the recombination.

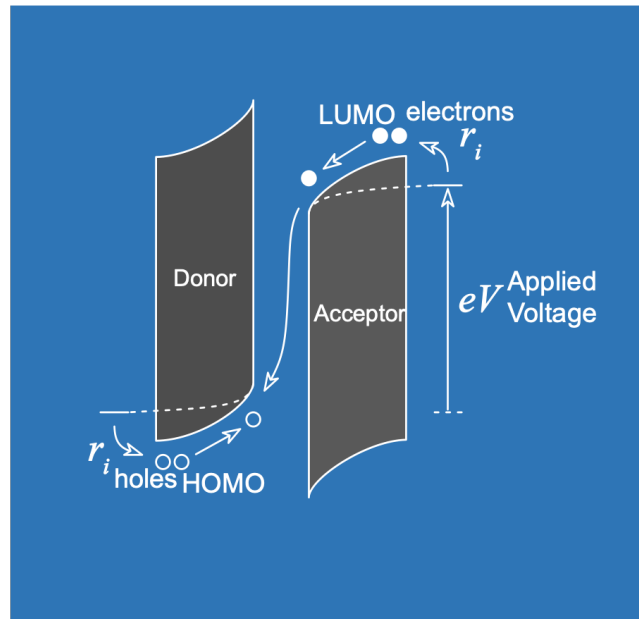


Figure 1-17: A Band Diagram above Injection

As applied voltage increases, the bands will keep shifting into a general positive slope, as Figure 1-17 shows. In this regime, the injection of charge carriers into the bands will be much easier and the recombination can happen quickly at the interface, so that the current becomes limited by the rate that charges can move along the bands. Therefore, after the Recombination Region, the dominant charge transport mechanism turns into space charge limited current with traps again.

We call this space charge limited current with traps region above injection the Transport Region to distinguish from the space charge limited current with traps below injection (Shunting Region). We would expect the voltage dependence of the Transport Region to be similar to that of the Shunting Region, because they both depend on traps. At the same time, we also expect a small difference between their voltage dependence, because the voltage dependence in Shunting Region is the mixture of non-radiative recombination and space charge limited current with traps,

while we could view the Transport Region as purely space charge limited current, for the voltage dependence of the Recombination Region is significantly different from that of the Transport Region. Therefore, compared to Shunting Region, we usually use Transport Region to study the space charge limited current with traps[5].

As the applied voltage keeps increasing, more carriers will enter the band. When almost all the traps are filled, the charges in the band will behave ohmically like a resistor again. Note that the Ohmic Region above injection has a much larger current compared to the Ohmic Region below the injection, though both have the same voltage dependence, because charges are now transporting along bands instead of moving through the disordered defects and filaments inside the materials. People also view the Ohmic Region above injection as effect of series resistance in our device.

### **Voltage Dependence in Photocurrent**

Similar to dark current, the movement of photocurrent is also determined by the shape of the energy bands. One big difference between photocurrent and dark current is that photocurrent is composed of the electron-hole pairs of charge carriers generated by the photovoltaic effects, instead of the charges injected by the electrodes. From the photovoltaic effects, the electrons and holes will enter the energy bands directly powered by the optical energy.

The photocurrent is equal to the number of electron and hole pairs produced by the photovoltaic effect from the incident light that are collected at the electrodes. Unlike dark current, the generation of the photocurrent will not change at different applied voltages. Thus, we do not need to worry about the limitation of charge transport caused by the significant change of the number of carriers. However, the fact that generated electron-hole pair could be at either the donor layer or the acceptor layer makes the photocurrent transport mechanisms more complicated. In this introduction, I will keep things simple and only discuss the direction of charge movement in photocurrent.

In a typical photocurrent IV curve, the first region is a constant negative current, as shown in Figure 1-8. This is when the band is tilted downward, as shown in

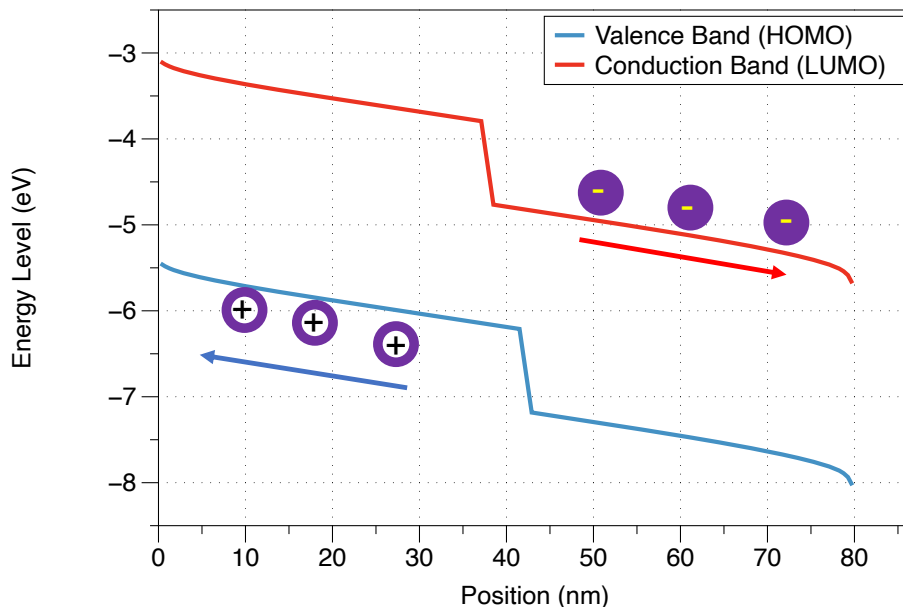


Figure 1-18: A Band Diagram for photocurrent below Injection

Figure 1-18. The dark current is always positive, and the positive electrode (anode) next to the donor layer collects electrons, and the negative electrode (cathode) next to the acceptor layer collects holes. When the bands are tilted downward at low applied voltage, the electron-hole pair generated by the photovoltaic effect will enter the bands and flow along with the band automatically—electrons move downward to the cathode, and holes move upward to the anode, producing negative current. Therefore, at the low voltage region, the photocurrent is opposite to the direction of the dark current.

As shown in Figure 1-19, the bands become roughly flat at higher applied voltage, near the compensation voltage. At this point, the photocurrent is expected to be zero, because charges have the same probability of moving to the left or right, and they do not know which direction to go.

When we enter the voltage above injection, the bands are tilted upward. The electrons will move downward to the left and the holes will move upward to the right, as shown in Figure 1-20. Even if the electron hole pair is split, the carriers will move in the direction of the dark current.

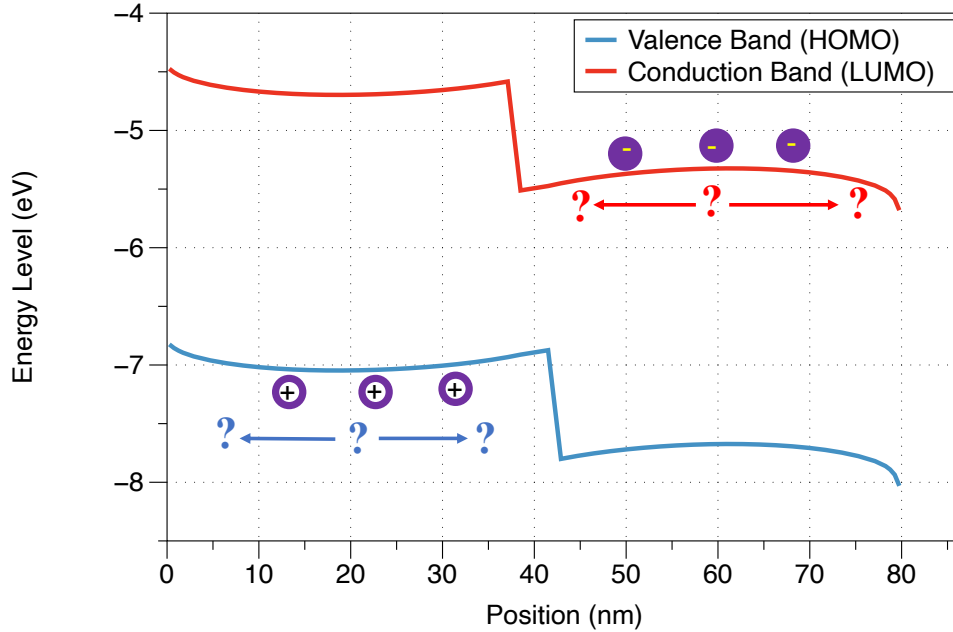


Figure 1-19: A Band Diagram for photocurrent around Injection

### 1.3.4 Circuit Diagram and Mathematical Formula

In section 1.3.2, we learned about different charge moving mechanisms for dark current and photocurrent at various applied voltages. Our analytical model tries to summarize these physics into a mathematical expression that could directly fit the data.

Previous work in the lab mainly focused on the behavior of dark current. There are five different charge transport mechanisms in solar cells' dark current: Ohmic region, Shunting Region, Recombination Region, Transport Region, and Ohmic region again. Figure 1-21 summarizes the physical locations of these mechanisms. Recombination happens at the interface between donor and acceptor. Transport takes place in either donor or acceptor. In Figure 1-21, Shunting is represented by its non-radiative recombination at the interface, although we know that charges need to go to interface for that. We use Transport to represent the space charge limited current with traps in general. Shunt resistance (Ohmic below injection) is inside the solar cell and series resistance (Ohmic above the injection) is outside of the solar cell.

We put the five different voltage-dependent mechanisms in a circuit diagram to demonstrate their contributions to the dark current, as shown in Figure 1-22. In the

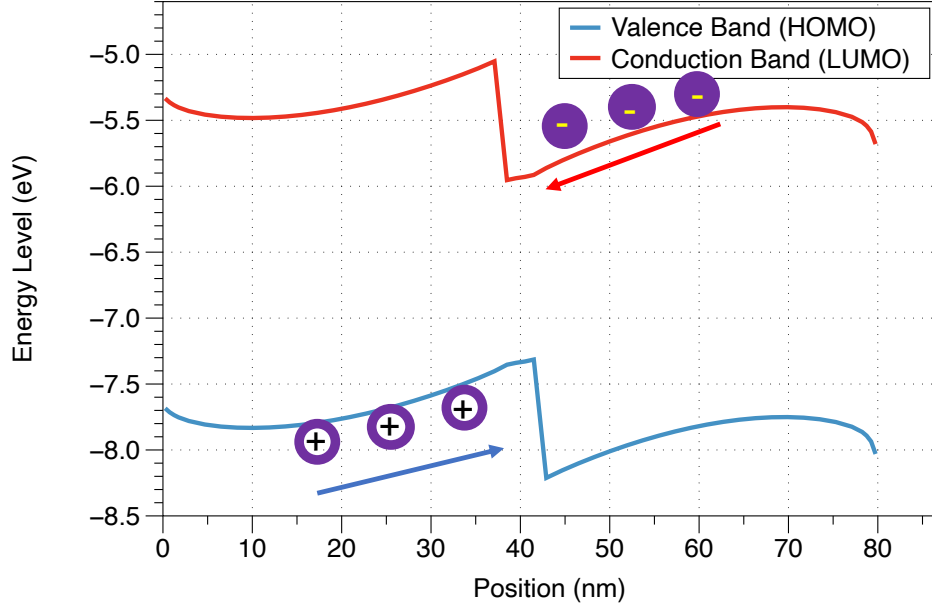


Figure 1-20: A Band Diagram for photocurrent above Injection

circuit diagram, the shunt resistance and series resistance are constant resistances, while the rest of the components are voltage-dependent rates. The current contributions that are in one pathway are put in series. For example, a carrier must go through transport to get to the recombination, and the higher resistance one for that voltage dominates that series pathway. The contributions that are not in one pathway are in parallel.

Based on the circuit diagram, we could combine each mechanism's contribution into a single mathematical formula for current in solar cells. However, due to the complexity of the equation, I will write the current at different voltage-dependent segments separately.

$$J_{ohmic} \propto V \tag{1.18}$$

$$J_{shunt} \propto V^B \tag{1.19}$$

$$J_{recomb} \propto V^M \tag{1.20}$$

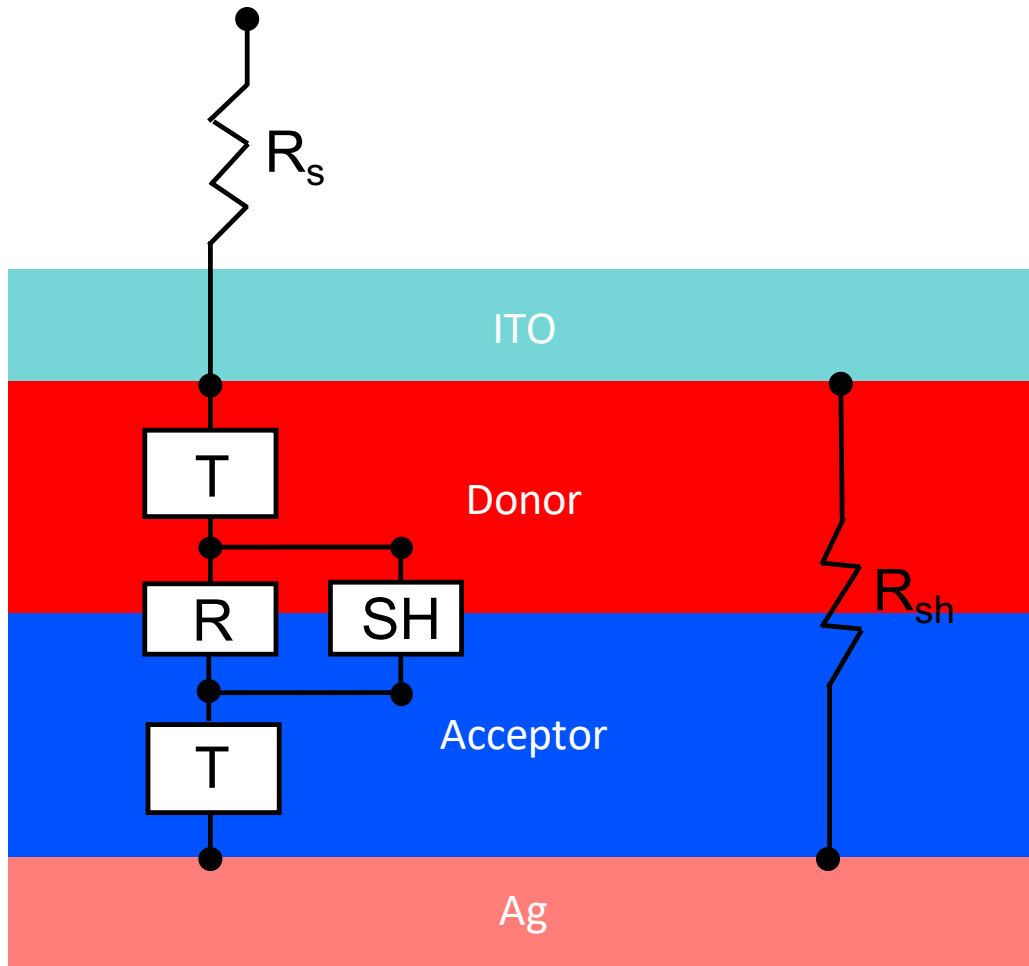


Figure 1-21: The Physics of Different Contributions

$$J_{transport} \propto V^N \tag{1.21}$$

Equation 1.18 refers to the ohmic current for both series resistance and shunt resistance. Equation 1.19, Equation 1.20, and Equation 1.21 are the currents due to Shunting, Recombination, and Transport mechanisms. Proportionality is used to demonstrate current terms. Of course, there are coefficients and offsets for each term when we use these equations to fit the data.

Following the circuit diagram in Figure 1-22, we add contributions together in either series or parallel. When the voltage is low, the rate of charge transport depends on the shunt resistance. Then, the rate of shunting region (SH) will increase and become the dominant channel (note that an increased rate is a smaller effective

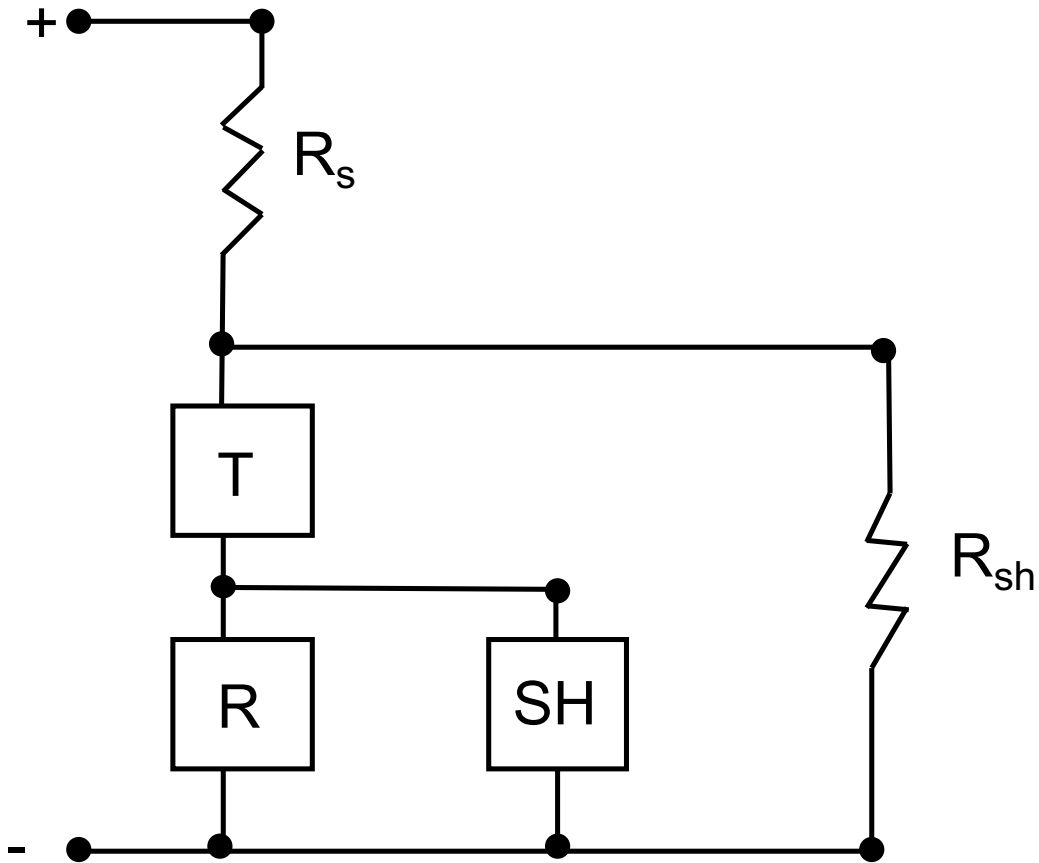


Figure 1-22: Circuit Diagram for Charge Transport Mechanisms in Dark Current

resistance at that voltage). After that, the rate of recombination ( $R$ ) will increase to dominate the charge transport. First, the recombination ( $R$ ) is the limiting factor, and as more carriers reach the interface and the recombination rate increases, the transport rate ( $T$ ) becomes the limiting factor. Finally, the series resistance will make the voltage dependence ohmic again. What I present is our best understanding of dark current right now. The equations of dark current are still under investigation and development, as we will discuss more in later chapters.

Figure 1-23 shows a typical fit by applying the dark current equation. We could see the current transport mechanisms are represented by five segments, which demonstrates their dominant regions at different applied voltages. The graph is log-log, so the slopes of these segments are equal to the powers of voltage in the linear-linear

equation. Thus, the slope of each segment reflects the voltage dependence of that region. We call the relationship between the slope, power, and voltage dependence as the power law, which is the foundation of our analytical model. In Figure 1-23, we observe that the voltage dependence (slope/power) is the highest for the Recombination Region, and the lowest for the Ohmic Region. The voltage dependence can provide useful information about the physics of the corresponding region. We are most interested in the voltage dependence of the Recombination Region, which we believe is related to the energy difference at the interface [13]. We also would like to investigate the voltage dependence of the Transport Region, which provides information about the trap distribution in our devices [12].

In summary, we have some understandings and expectations about the charge transport mechanisms of dark current and photocurrent. However, our existing model centers on the dark current and has not incorporated the photocurrent into the mathematical expression yet. This thesis will discuss our work on better understanding the photocurrent and how we unify photocurrent and dark current into a complete model.

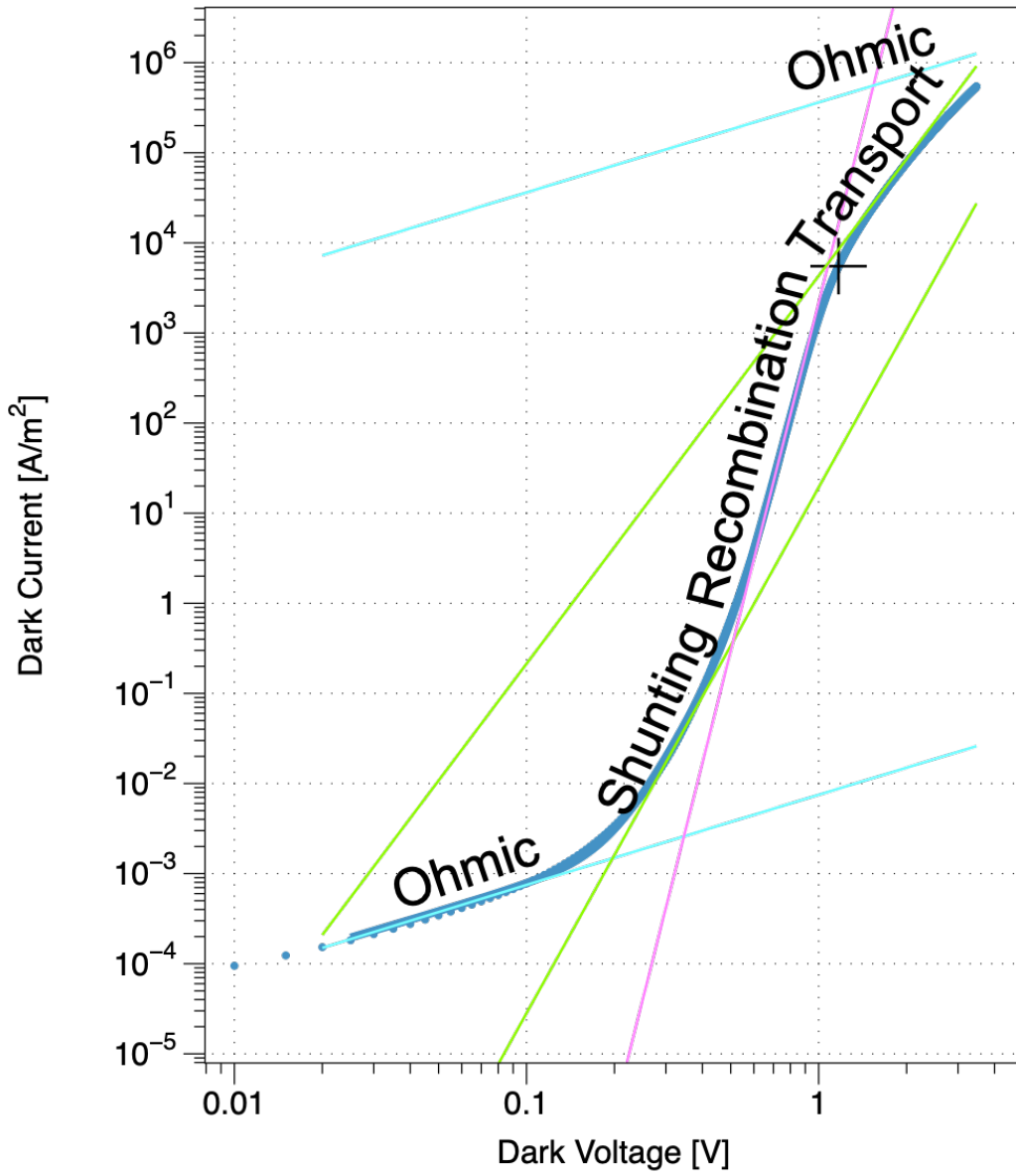


Figure 1-23: A Typical Fit for Dark Current using our Analytical Model



# Chapter 2

## Techniques

In this chapter, the techniques we use to investigate our analytical model for current in solar cells will be discussed. I will introduce why we would like to use simulation, how to use the simulation, and several important functions of the simulation. After that, I will discuss how we apply our analytical model of current in solar cells to the simulation.

### 2.1 Solar Cells in GPVDM simulation

We use an existing simulation package called GPVDM (general purpose photovoltaic device model), created by Roderick MacKenzie, to study the current in solar cells [26].

There are many benefits of using simulation to study the current. First, we could control over more parameters of the solar cells in simulation compared to the fabrication in lab. For example, in the simulation, we could set the energy difference between donor and acceptor to be any value we want, but in experiments, we can only use the energy difference from available materials. Another example is that measuring traps, mobility and all the other parameters requires additional experiments and the results might not apply to all solar cell structures, while we could adjust these electrical parameters easily in simulation.

Second, simulation can avoid the imperfections in the experiments. It is impossible

to make the fabrication process entirely ideal during the experiments, so we need to worry about defects in the devices, such as the crystallization at the surface of the sample. The devices that are produced at multiple times may have different behaviors due to slight differences in the fabrication process. However, this problem does not exist in the simulation, because we could always reproduce a simulation easily by setting all the parameters as the same. Because of the stability and reliability, it is good to use simulation to explore the theoretical hypothesis, such as our analytical model for current in solar cells. Moreover, we view simulation as a preparation for our future experimental work.

Additionally, the simulation can be used as a complementary way to understand the experimental results. We are trying to use the GPVDM to reproduce the results we got from experiments and examine what parameters give us the results. This could help us guess the parameters of the experimental devices that could not be measured directly, such as the carrier density and mobility.

At the same time, we have to acknowledge that there are some limitations of the simulation compared to experiments.

First, the simulation software is based on many assumptions, and these assumptions might be incorrect or incomplete. We will discuss more about incomplete assumptions later.

Next, the difference between the simulation and the experiments always exists. In the previous paragraphs, we view the fact that the simulation could not capture some fabrication imperfection as a benefit. However, it also means that even if the simulation works well, it may not be able to capture certain defects that determine how a device works realistically. So, the simulation always needs to combine with experiments to generate practical conclusions.

As we have discussed before, we study bilayer planar organic semiconductor solar cells, and we would like to reproduce the same devices in the simulation. However, due to the shortcomings of the simulation software, GPVDM, we made several changes to the device structure.

Most importantly, we change the device from a two-layer device to a three-layer

device, because GPVDM doesn't catch the physics of recombination at the interface properly. Most researchers use GPVDM to simulate single layer blend bulk heterojunction solar cells. For bulk heterojunction solar cells, the geometry of the interface is unknown as the materials are more mixed together to create a corrugated interface. Therefore, GPVDM implements the effective medium approximation where the device is treated as a single layer with a band gap equation to the energy difference at the interface. This effective medium allows recombination to happen at all locations in the device, not just at the interface. Since we are particularly interested in the physics of the interface, we would like to use bilayer solar cells with a well defined interface, but GPVDM does not allow for recombination across the interface.

We have contacted the designer of the GPVDM, Rod MacKenzie, to discuss this problem, and Rod adds free to free carrier recombination across the interface. However, we still need the free to trap recombination across the interface. We are working with Rod to think about how to add that to GPVDM. Now, we include the physics of interfacial recombination by manually adding an artificial third layer in between the donor and acceptor layer. We choose the thickness of the middle layer to be 4 nm and set it to have the same electrical properties as both donor and acceptor, which will be explained with more details in [Figure 2-2](#).

In addition to the third layer, another modification is that we use a symmetric device in simulation instead of the asymmetric experimental device. Specifically, we set the thickness, the light absorption, the mobility, and all the other parameters besides the energy difference between donor and acceptor to be identical. More about these parameters will be discussed in the next section. In other words, we set all the parameters other than the one that we would like to investigate as the same, which will make our comparison more convenient. We believe that using symmetric devices will not affect the reliability of our generic conclusions, and the symmetric devices allow us to start from a simple point to understand the whole complicated scenario.

## 2.2 Basic Settings and Default Simulation

There are many settings that we need to choose for GPVDM simulation.

We figured out the reasonable values for each parameter in GPVDM after exploring them for several months by looking at the qualitative behaviors of the IV output and checking values in the literature [27]. We would like the input parameters to be comparable with the parameters for real devices.

Below are the “default” parameters and basic settings we choose for our bilayer solar cells. There is still a lot of space for improvements and adjustments on those settings. Others in our lab are working on using experimental data to extract the simulation parameters for GPVDM.

Layer name	Thicknes	Optical material	Layer type	Solve optical problem	Solve thermal problem
ITO	1e-07	... oxides/ito	contact ▼	Yes ▼	Yes ▼
Donor	3.8e-08	... generic/generic_organic	active layer ▼	Yes ▼	Yes ▼
middle	4e-09	... generic/generic_organic	active layer ▼	Yes ▼	Yes ▼
Acceptor	3.8e-08	... generic/generic_organic	active layer ▼	Yes ▼	Yes ▼
Al	1e-07	... metal/al	other ▼	Yes ▼	Yes ▼

Figure 2-1: The Structure of Layers in Solar Cells.

First of all, we need to set the structures of our devices. As we have discussed before, we simulate symmetric devices with the donor layer, middle layer, and acceptor layer. Figure 2-1 shows the structure, in which the first column tells us the name for each layer. Notice the thickness of each layer (in the second column) are set to 100 nm, 38 nm, 4 nm, 38 nm, and 100 nm. In real experiments, the donor layer is usually 20 nm, and the acceptor layer is 40 nm. In the default simulation, we set the thickness of both acceptor and donor as 40 nm for symmetry. Then, we add a 4 nm middle layer in the middle, and the donor and acceptor layers become 38 nm. In addition to the three layers, we have two layers of electrodes, which are labeled as ITO and Al. The two electrodes are named after the materials of the electrodes in real experiments, although in the simulation, the only property of electrodes that

matters is whether it's a hole electrode or electron electrode. Similar to the setting of electrodes, we didn't set the optical material to be specific to a type of material, because we would like to investigate the general behaviors.

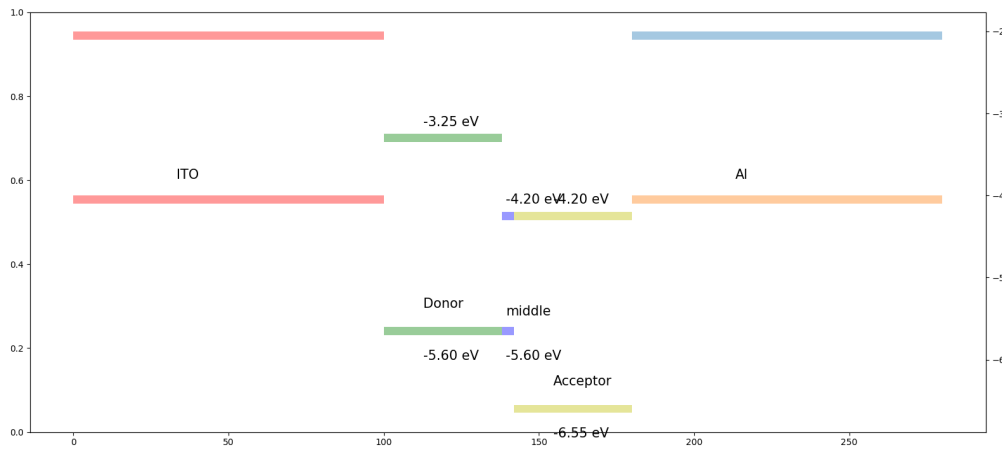


Figure 2-2: The Energy Level for Donor, Middle, and Acceptor Layers in a Default Simulation.

After selecting the structure of the device, the next step is to figure out the electrical parameters. The electrical parameters that we are most interested in are the energy level of the donor and acceptor. For the donor layer, we used the energy level of SubPC (the donor material that we usually use in experiments), which has LUMO as -3.25 eV and HOMO as -5.6 eV. For the acceptor layer, we started with the LUMO for C<sub>60</sub> (the acceptor material that we usually use in experiments), which is -4.2 eV. However, in order to create symmetric devices, we set the HOMO of the acceptor to be -6.35 eV, so that the difference between HOMO and LUMO for a single layer is the same for donor and acceptor, and the barrier encountered by electrons and holes are symmetric at the interface. In this case, the energy difference between the HOMO of the donor and the LUMO of the acceptor is 1.4 eV. For the middle layer, we set its LUMO to be -4.2 eV and its HOMO to be -5.6 eV, so that it aligns with the energy levels for the donor and acceptor. Figure 2-2 shows the energy levels for each of the donor, middle, and acceptor layers clearly, which are sitting in between two electrodes.

DoS of Donor		
DoS distribution	<input type="radio"/> Exponential	Edit
Electron trap density	<input type="text" value="5.4000e24"/>	$m^{-3} eV^{-1}$
Hole trap density	<input type="text" value="5.4000e24"/>	$m^{-3} eV^{-1}$
Electron tail slope	<input type="text" value="0.15"/>	eV
Hole tail slope	<input type="text" value="0.15"/>	eV
Electron mobility	<input type="text" value="1e-06"/>	Symmetric $m^2V^{-1}s^{-1}$
Hole mobility	<input type="text" value="1e-06"/>	Symmetric $m^2V^{-1}s^{-1}$
Relative permittivity	<input type="text" value="3.0"/>	au
Number of traps	<input type="text" value="5"/>	bands
Free electron to Trapped electron	<input type="text" value="1.0000e-21"/>	$m^{-2}$
Trapped electron to Free hole	<input type="text" value="1.0000e-21"/>	$m^{-2}$
Trapped hole to Free electron	<input type="text" value="1.0000e-21"/>	$m^{-2}$
Free hole to Trapped hole	<input type="text" value="1.0000e-21"/>	$m^{-2}$
Effective density of free electron states (@300K)	<input type="text" value="5.0000e25"/>	$m^{-3}$
Effective density of free hole states (@300K)	<input type="text" value="5.0000e25"/>	$m^{-3}$
$\chi_i$	<input type="text" value="3.25"/>	eV
$E_g$	<input type="text" value="2.35"/>	eV
$n_{free}$ to $p_{free}$ Recombination rate constant	<input type="text" value="0.0"/>	$m^3s^{-1}$
Free carrier statistics	Maxwell Boltzmann - analytic	type

Figure 2-3: The electrical parameters for the donor layer in a default simulation.

DoS of middle		
DoS distribution	<input type="radio"/> Exponential	Edit
Electron trap density	<input type="text" value="5.4000e24"/>	$m^{-3} eV^{-1}$
Hole trap density	<input type="text" value="5.4000e24"/>	$m^{-3} eV^{-1}$
Electron tail slope	<input type="text" value="0.15"/>	eV
Hole tail slope	<input type="text" value="0.15"/>	eV
Electron mobility	<input type="text" value="1e-06"/>	Symmetric $m^2V^{-1}s^{-1}$
Hole mobility	<input type="text" value="1e-06"/>	Symmetric $m^2V^{-1}s^{-1}$
Relative permittivity	<input type="text" value="3.0"/>	au
Number of traps	<input type="text" value="5"/>	bands
Free electron to Trapped electron	<input type="text" value="1.0000e-21"/>	$m^{-2}$
Trapped electron to Free hole	<input type="text" value="1.0000e-21"/>	$m^{-2}$
Trapped hole to Free electron	<input type="text" value="1.0000e-21"/>	$m^{-2}$
Free hole to Trapped hole	<input type="text" value="1.0000e-21"/>	$m^{-2}$
Effective density of free electron states (@300K)	<input type="text" value="5.0000e25"/>	$m^{-3}$
Effective density of free hole states (@300K)	<input type="text" value="5.0000e25"/>	$m^{-3}$
$\chi_i$	<input type="text" value="4.2"/>	eV
$E_g$	<input type="text" value="1.4"/>	eV
$n_{free}$ to $p_{free}$ Recombination rate constant	<input type="text" value="0.0"/>	$m^3s^{-1}$
Free carrier statistics	Maxwell Boltzmann - analytic	type

Figure 2-4: The electrical parameters for the middle layer in a default simulation.

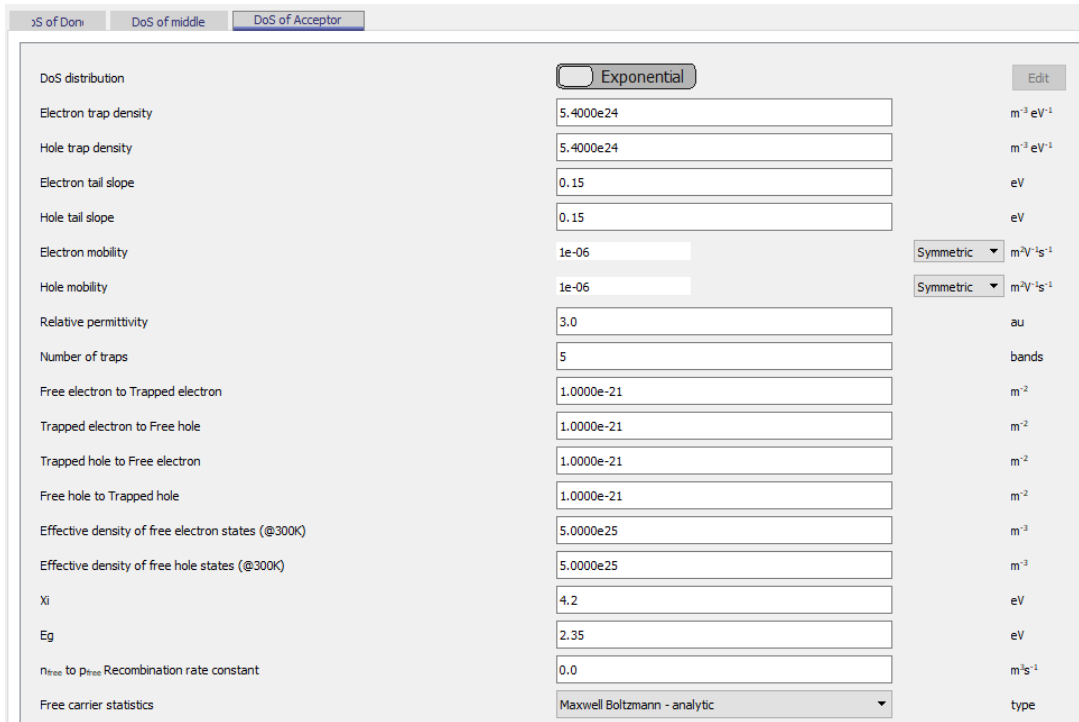


Figure 2-5: The electric parameters for the acceptor layer in a default simulation.

Figure 2-3, 2-4, and 2-5 illustrate the electrical settings for three layers, in which Xi and Eg are LUMO and the difference between LUMO and HOMO for each layer. We set all the electrical parameters other than the energy levels to be the same, selected from our initial exploration of reasonable parameters.

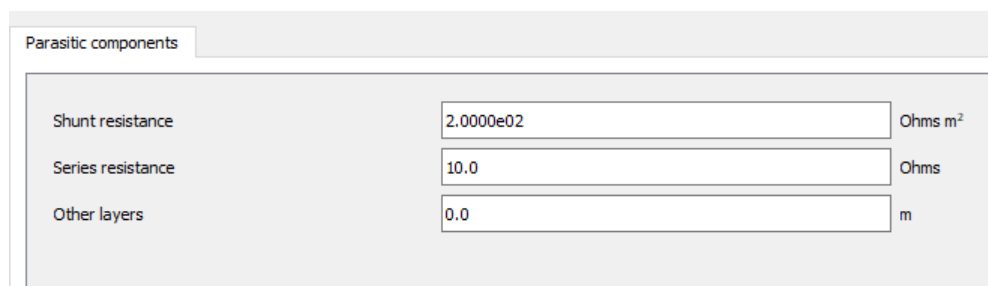


Figure 2-6: The Shunt Resistance and Series Resistance of a default simulation

We also need to set the shunt resistance and series resistance for our device. We choose our shunt resistance to be  $200 \Omega m^2$  and series resistance to be  $10 \Omega$ , as shown in Figure 2-6. Recall that the series resistance and shunt resistance are fundamental parts of the circuit diagram, such as shown in Figure 1-22.

Name	Top/Bottom	Applied voltage	Charge density/ Fermi-offset	Majority carrier	Physical model	ID
top	top	Change Vsig	5e25 m <sup>-3</sup> / -0.00 eV	Hole	Ohmic	...
btm	bottom	Constant bias 0.0	5e25 m <sup>-3</sup> / -0.00 eV	Electron	Ohmic	...

Figure 2-7: The settings of electrodes in a default simulation

Then, we need to figure out the settings of electrodes. By selecting an electrode as a hole majority carrier, the offset is set relative to the HOMO. For electrons, the offset is relative to the LUMO. Because we only need to keep things symmetric, we set the offsets for two electrodes to be both 0 as shown in Figure 2-7. This means we set the carrier concentration at the electrodes to have ohmic contacts and no barriers.

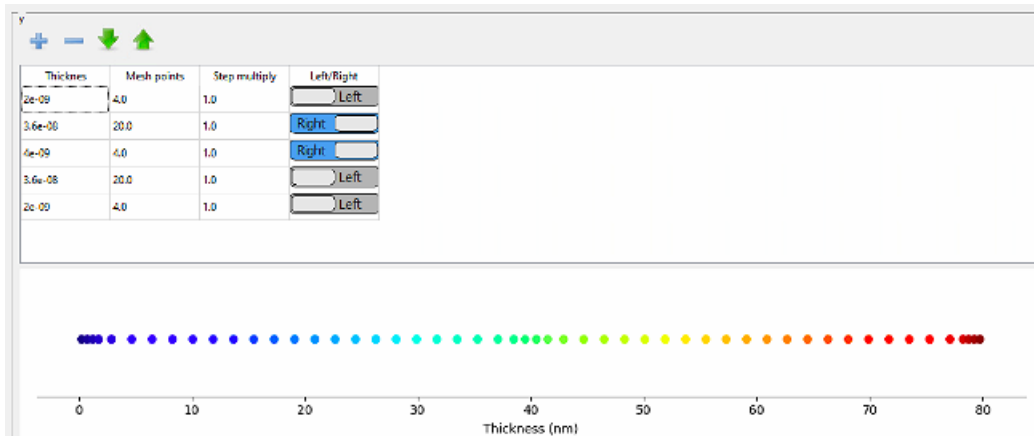


Figure 2-8: Electrical Mesh Points in a default simulation

Moreover, we need to set the electrical mesh points for our default device. The GPVDM simulation is based on solving differential equations inside the solar cells. The electrical mesh points are related to how we solve the differential equation for the simulation. Fewer mesh points make it faster to solve the differential equations, while more mesh points could provide more details. It is contradictory that we would like to have less mesh points to depict the physics with more details. Thus, we try to find a compromise between more points and fewer points, and our decision in the default device is shown in Figure 2-8. We set more points at the electrodes and the interface, where we would like to observe the rapid change of carrier concentration and other

parameters over space. We set relatively fewer mesh points across the donor and acceptor layers, because we believe the physics there is more uniform.

## 2.3 Output in GPVDM

### 2.3.1 Dark JV curve and Light JV curve

The most important result we could get from the GPVDM is the JV curve. GPVDM allows us to change the light intensity in a simulation. When we set the light intensity to be 0, the generated JV curve is the dark current. When we set to light intensity to be 1 (in the unit of sunlight), GPVDM generates the light current. It is also possible to change the light intensities to 0.01, 0.1 or 10, and we could use GPVDM to investigate the behavior of a device under different light intensities. However, when we are not investigating the different light intensities, our default light intensity for devices is 1.0.

### 2.3.2 Finding the True Compensation Voltage

GPVDM has a useful output called snapshots, which allows us to examine many parameters across the device at different applied voltages.

As we have mentioned in Section 1.2.4, compensation voltage is equal to the flat band voltage. The snapshots give us a chance to directly extract the flat band voltage from GPVDM. There are two important parameters in snapshots: band diagram and potential.

The energy band diagram is what we have introduced in the previous chapter. GPVDM displays the conduction band, valence band, quasi Fermi level for holes, and quasi Fermi level for electrons as  $E_c$ ,  $E_v$ ,  $F_p$  and  $F_n$ . The Figures 2-9, 2-10, and 2-11 are examples of the band diagrams provided by GPVDM.

Comparing the energy band diagram at different applied voltages, we notice the general slope of the energy band is changing from negative to positive. The trend becomes more obvious, when we plot the band diagram for multiple voltages together,

as illustrated in Figure 2-12. However, it is difficult to find the flattest band voltage directly from the band diagrams, because the “flat” here is not a simple horizontal line, but the curvature with a general slope of zero.

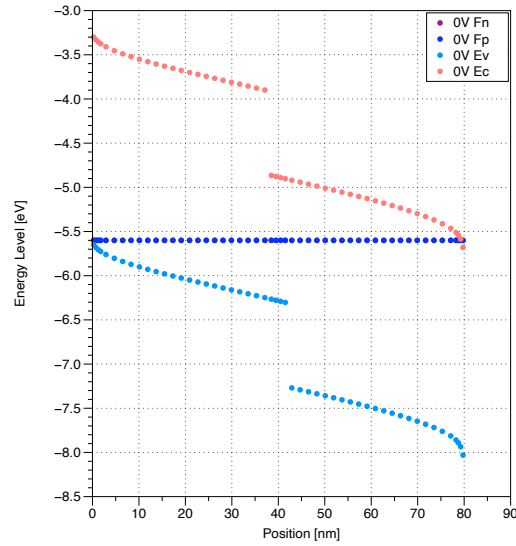


Figure 2-9: The band diagram in GPVDM at 0 applied voltage. Ev, Ec are valence band and conduction bands. Fn, Fp are quasi Fermi levels. The general slopes of the valence band and conduction band are negative.

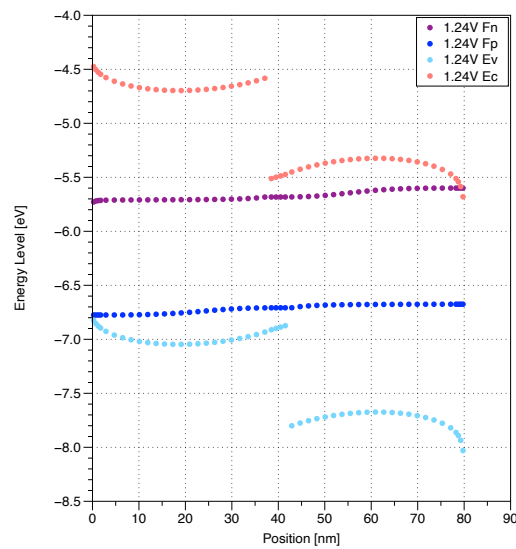


Figure 2-10: The band diagram in GPVDM at 1.24 applied voltage. The valence band and conduction band are roughly flat.

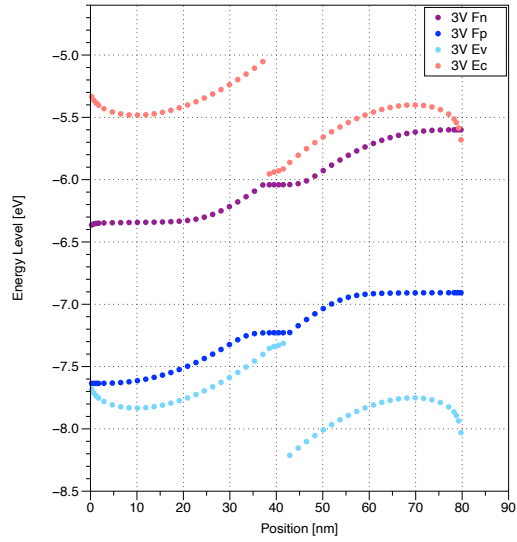


Figure 2-11: The band diagram in GPVDM at 3V applied voltage. The general slopes of the valence band and conduction band are positive.

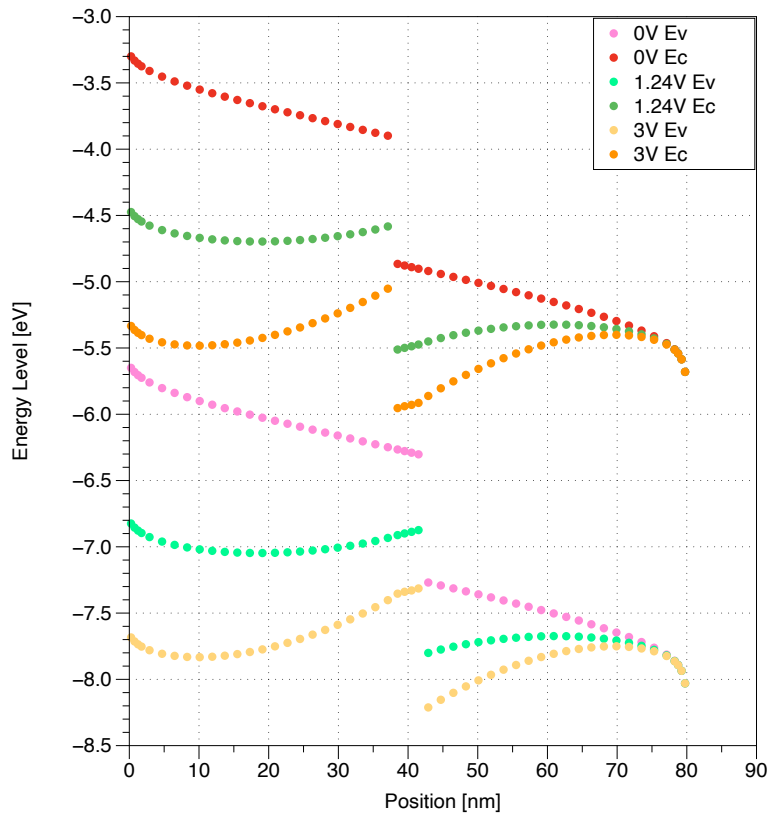


Figure 2-12: The conduction bands and valence bands for device at 0V, 1.24V, and 3V applied voltages in GPVDM.

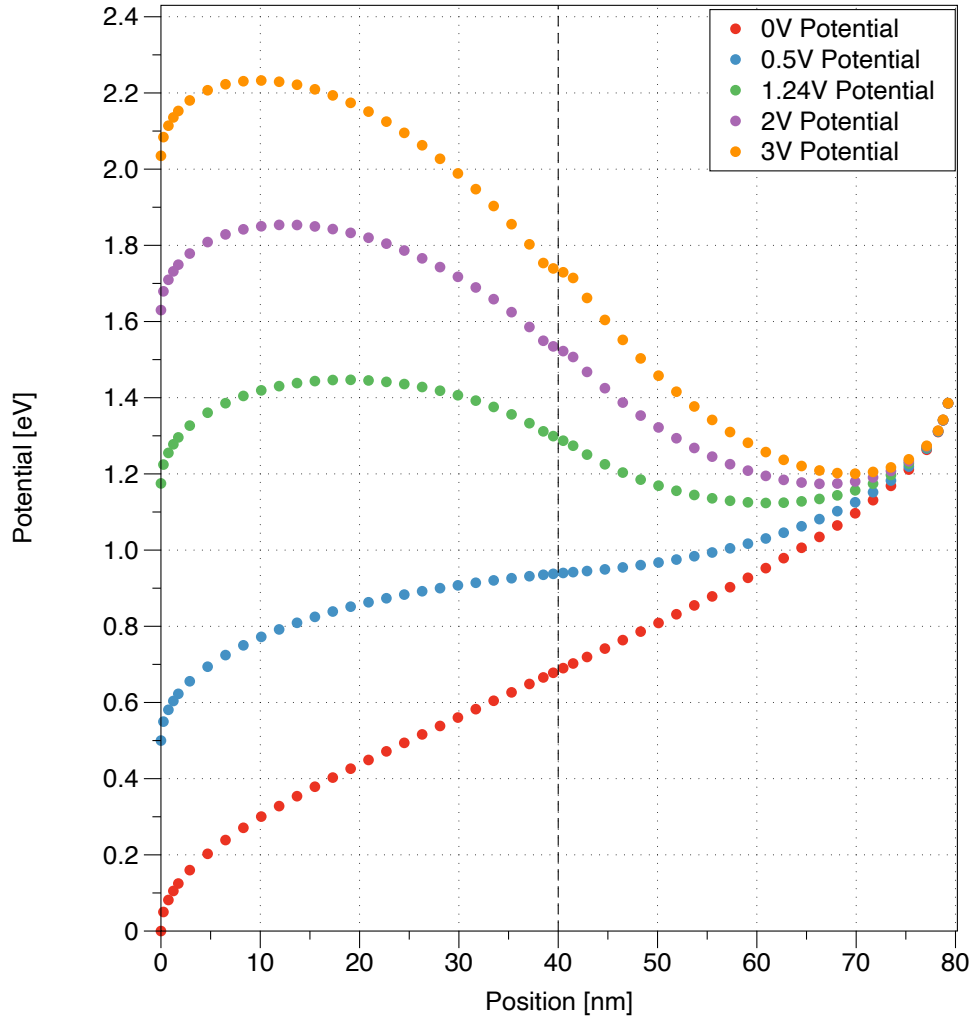


Figure 2-13: The plot of potential from GPVDM at different applied voltages.

Another parameter in snapshots called potential allows us to find the flat band voltage in a more straightforward way. The potential is a value that could be calculated from the energy band diagram, and the potential describes how the conduction band shifts from the conduction band at zero applied voltage, as shown in Figure 2-13. Similar to the general slopes of bands, we observed that the shape of potential also changes at different applied voltages, varying from positive slope to flat and to negative slope. After more investigation, we realized that the applied voltage where the shape of potential curve is flat is identical with the applied voltage that makes the band diagram flat.

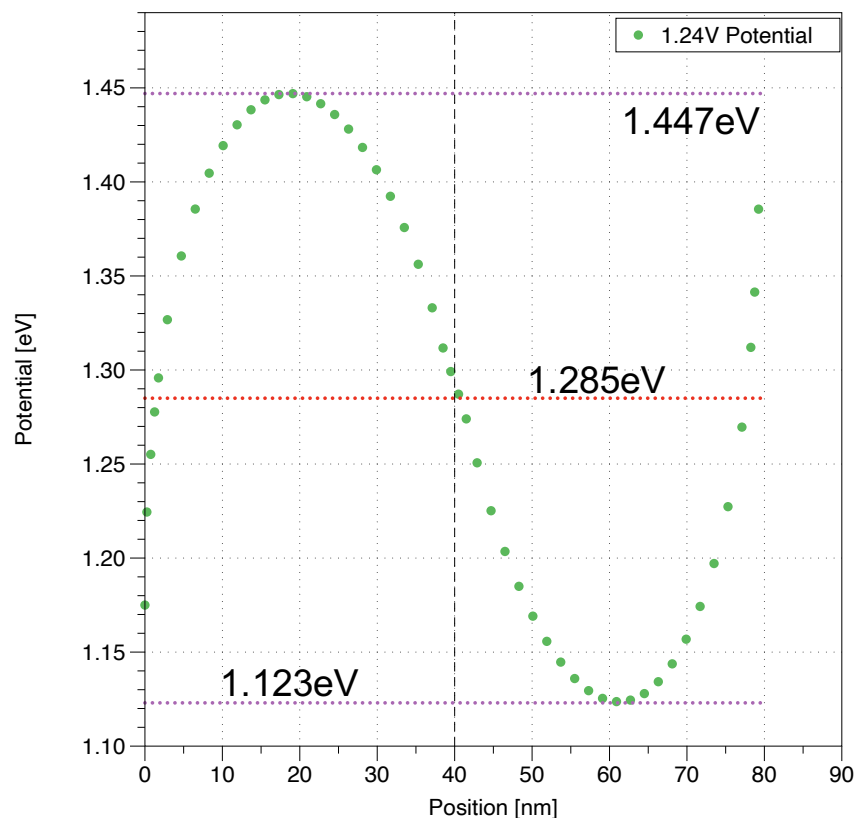


Figure 2-14: Potential plot at the compensation voltage, where the left point is equal to the middle point is equal to the right point as shown by the dashed line of 1.285 eV.

Thus, we figure out the method of using the potential snapshot to extract compensation voltage directly from GPVDM: when the potential at the left is equal to the potential at the middle point, and it's equal to the potential at the right, the corresponding applied voltage here is what we called as the compensation voltage, as shown in Figure 2-14. The data points near the edges are not important, because these points describe the boundary condition at the contacts rather than the physics of the donor and acceptor layers. Therefore, we would like to ignore the potential near the edges and compare the potentials that are 1 nm to 2 nm from the edges with the potential at the middle (40nm). We also expect the maximum and minimum potentials to be symmetric around the potential at the middle, as shown by the purple and red dashed lines in Figure 2-14.

### 2.3.3 Other characteristics that could be extracted from GPVDM

In addition to JV curves, energy band and potential, there are many other useful parameters of the device that could be extracted from the snapshots. For example, we could extract the carrier concentration of holes and electrons in both free and trapped states at different applied voltages.

## 2.4 Fitting the Simulation in Datagraph

After extracting the results from GPVDM, we usually use a plotting software called Datagraph to analyze them.

Standard curve fitting allows researchers to type in a function with multiple fit parameters, and standard algorithms will minimize the difference between the data and the function. Typically for complicated equations, initial guesses and constraints on the possible range of values are needed. Datagraph makes this process more straightforward by plotting the fit function and updating it as you use a “slider” to see how shifting a parameter affects the curve. In this way, the user can eyeball the fit before the algorithm takes over to optimize.

A general method of finding the initial value is to first set the initial guess in a large range of values and drag the “slider” to figure out a narrower reasonable range for that parameter. Then, we could first change the initial guess to that parameter and repeat the previous steps, using the slider to confine the range of initial guess, and we can figure out the most accurate initial guess easily. Although the slight change in initial guess usually does not matter for finding value of this specific parameter, we could adjust it anyway, because changing the initial guess to a specific number after you determine the range could make the fitting for other parameters more accurate.

Figures 2-15, 2-16, 2-17 describe a typical process of changing the initial parameters. In Figure 2-15, the function form is the equation we type in. For the unknown parameter, we check the “optimize” box. The value on the left is our initial guess and the value on the right is the fitting parameter generated by Datagraph. Let’s focus on the value of “f”. In Figure 2-15, the initial guess for “f” is 10, and the fitting value

for “f” is about 7.44. In Figure 2-16, we change the initial value to a number away from the reasonable range. We notice that the fitting fails here, because we expect “f” to be a positive number. In Figure 2-17, we change the initial value to a number closer to the real value, and the fitting adjusts the parameters by a little bit. Thus, it is always good for the fitting if we keep the initial values closer to the actual value. Notice that in the screenshots below, the “d” is set to be -0.08, which is our previous default “d”. In later section, the value of “d” will be modified into -0.115.

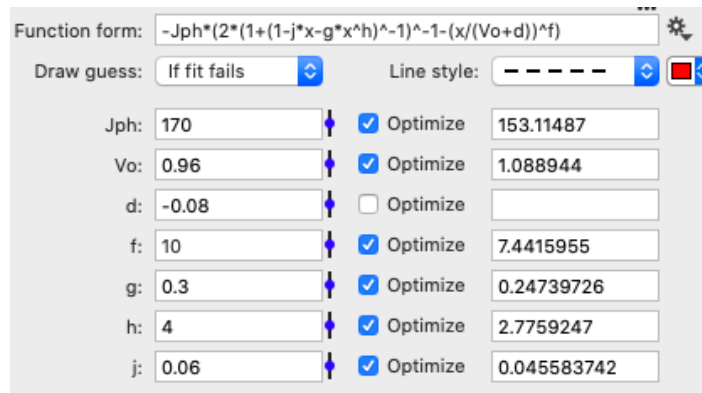


Figure 2-15: Fitting panel in Datagraph, setting the initial value for f as 10

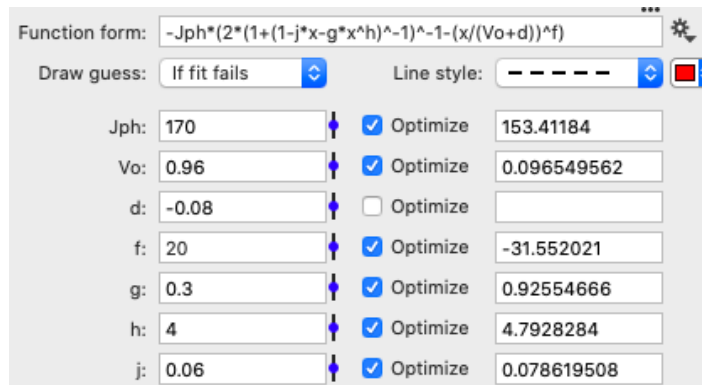


Figure 2-16: Fitting panel in Datagraph, setting the initial value for f as 20. Note the fit fails because f cannot be negative.

Another important tip for determining the initial guesses is that we could use the initial guesses from similar devices as a reference. If the devices are not very different from each other, we could usually use the same initial guesses for our devices. That’s another benefit for having a default device.

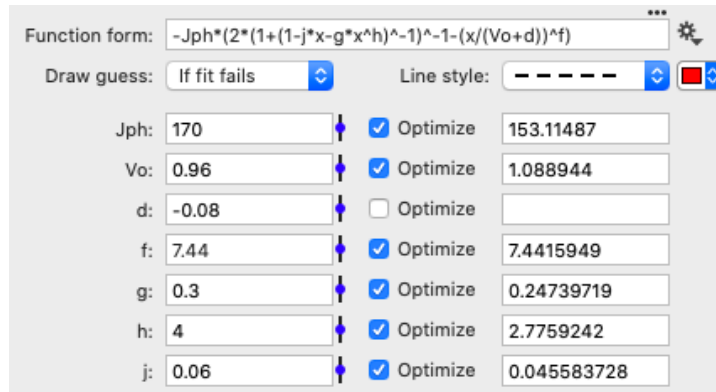


Figure 2-17: Fitting panel in Datagraph, setting the initial value for f as 7.44

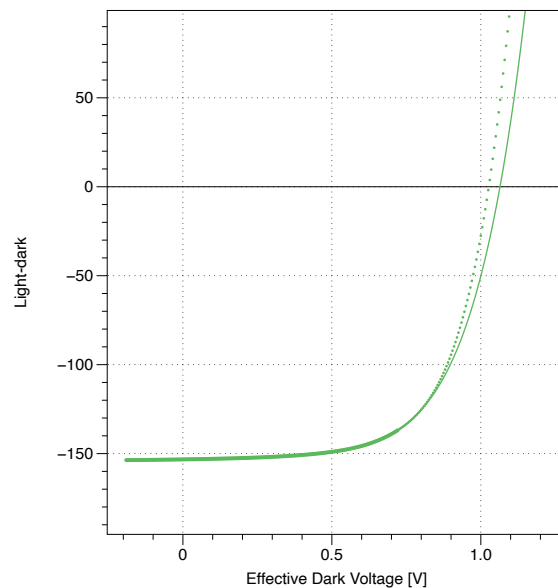


Figure 2-18: A bad fit of photocurrent. The fit range is from -0.2V to 0.725V.

For the data that we fit completely, such as the dark current, we are able to get a nice fit after setting the initial guesses properly. However, for the data that we only fit partially, such as photocurrent, we also need to adjust the fit range carefully to find the best fit for the curve. For example, the fit in Figure 2-18 is not an ideal fit, because there is obvious discrepancy between the data points and the fit curve. At this point, we need to adjust the constraints on fit range. Figure 2-19 is an example for the ideal fit curve that we will get when set the proper fit range. In Figure 2-19, we almost cannot tell the fit curve from original data.

In summary, GPVDM allows us to run the simulation of solar cells, and Datagraph

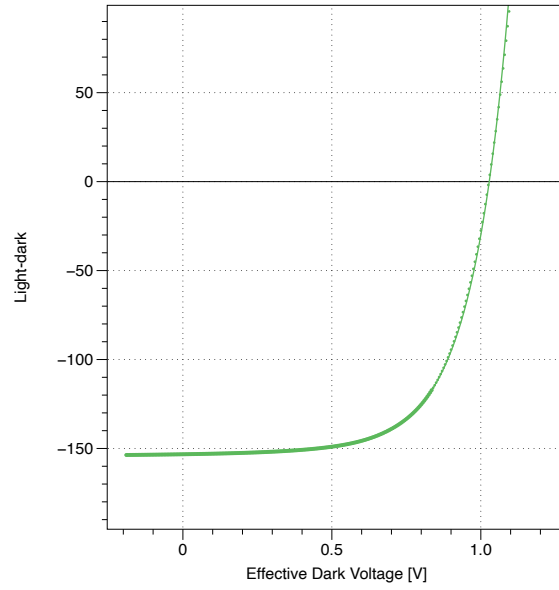


Figure 2-19: A good fit of photocurrent. The fit range is from -0.2V to 0.837V.

enables us to analyze the data from simulation. With the help from GPVDM and Datagraph, we are able to learn more about the current in solar cells. I will talk about our research on photocurrent in the next chapter.



# Chapter 3

## Photocurrent

In this chapter, I will present the development of our photocurrent model, including the original photocurrent equation, the correction of series resistance, the power law dependence, and the new photocurrent equation.

### 3.1 Original Equation for Photocurrent

As we have discussed before, compensation voltage is critical for characterizing the IV behavior of solar cells and the energy difference at the interface. We would like to extract the accurate compensation voltage from the photocurrent fit to study solar cells.

A common question is why we need a fit to find compensation voltage instead of extracting the compensation voltage directly from where the photocurrent is zero. This is because both light current and dark current increase rapidly near zero. The photocurrent is the difference between light current and dark current, so a relatively small change in the dark or light current could result in a significant change in photocurrent. Considering how accurate the measurements in lab could be, we do not trust the photocurrent near zero as much as the photocurrent at lower voltages.

Therefore, we would like to find out a fit that could give us the compensation voltage only from the low voltage region. Prior to this thesis, we used a sigmoid shape fit equation to extract compensation voltage from the photocurrent, as shown

below:

$$J_{photo} = \frac{-2a}{e^{(V-b)/c} + 1 + \frac{1}{1-fV}} \quad (3.1)$$

In the original photocurrent fit equation,  $J_{photo}$  is the current density and  $V$  is the voltage for the JV curve. Other variables are the fitting parameters that we are able to extract: “a” represents the magnitude of the photocurrent, “b” is related toward the voltages that photocurrent turns to zero, “c” suggests the curvature of the photocurrent, and “f” is related to the slope of the bottom part of the photocurrent. Considering from the perspective of the Fermi-Dirac distribution, “c” has the same role as the temperature.

This function allows us to control the curvature and slope of the bottom part of the curve, and Figure 3-1 shows us how the four parameters control different parts of the fit. Figure 3-1 also demonstrates that only the first part of the photocurrent fits perfectly with the fitting, while the rest of it only roughly matches with the fitting.

By fitting the photocurrent with Equation 3.1, we are able to extract the compensation voltage from the photocurrent fit with the a simple relation:

$$V_0 = b + e^c \quad (3.2)$$

in which,  $V_0$  is the compensation voltage, and “b” and “c” are fitting parameters. Equation 3.2 is entirely empirical, placing  $V_0$  near the expected value. In Figure 3-1, the compensation voltage we calculated from Equation 3.2 is marked by the “+” sign. Notice that we extracted the compensation voltage from the fitting curve instead of the data itself.

However, we need to keep in mind that everything related to the original photocurrent equation is an estimation from experience, which only provides us a guess for the compensation voltage.

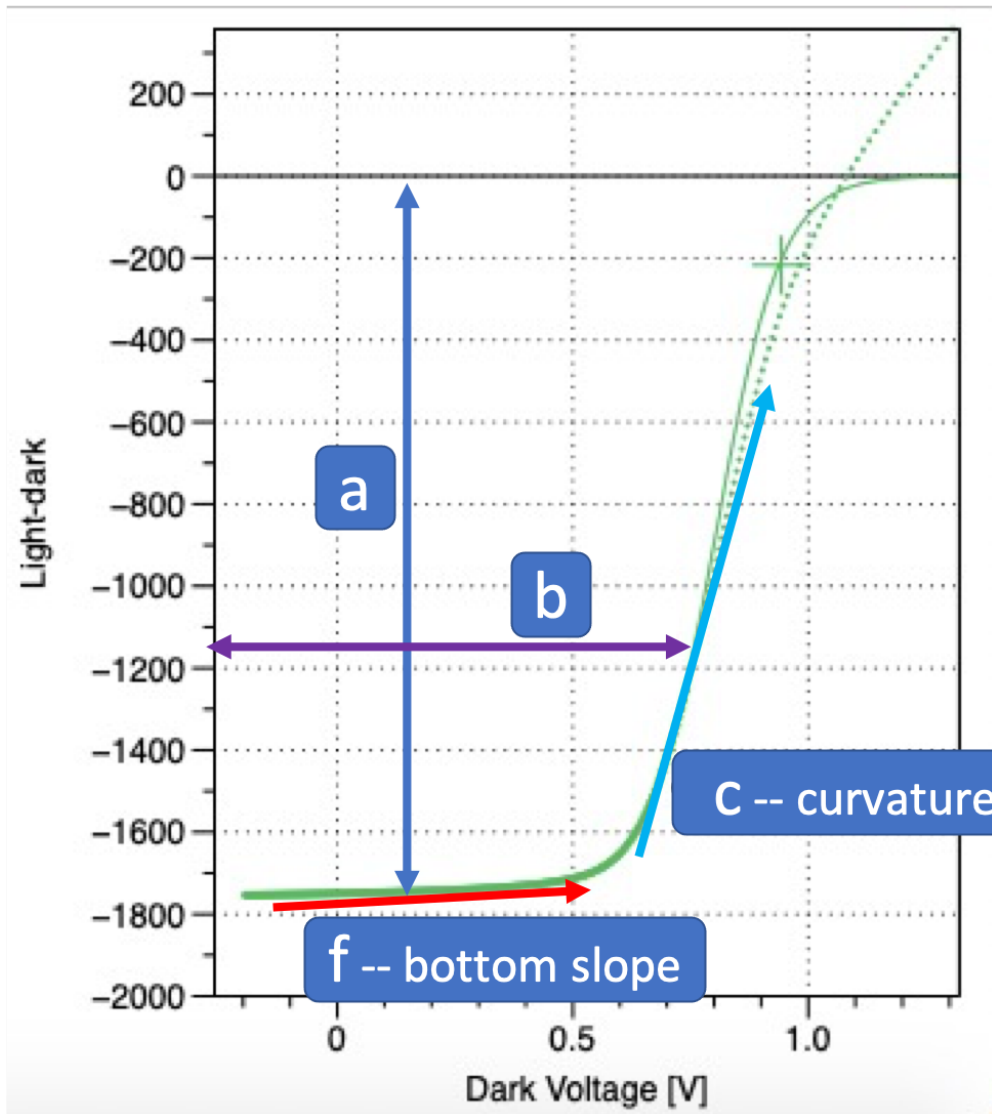


Figure 3-1: A typical original photocurrent fit with parameters a, b, c, and f

### 3.2 Correcting Voltage for Series Resistance

By reviewing the definition of photocurrent and reading related literature [23] [24], we found out there was a problem in our old method of extracting photocurrent—we did not take the series resistance into account.

Series resistance behaves like an ohmic resistance. It acts in series with the solar cell itself. In another word, the voltage is distributed between the series resistance and the solar cell itself, which means the series resistance and solar cell are separate. So, when we consider the voltage drop across the solar cell, we have to subtract the

voltage drop across the series resistance from the total applied voltage. The voltage drop across only the solar cell itself is called effective voltage, which is the equal to the difference between the total applied voltage and the voltage across the series resistance.

$$V_{effective} = V_{applied} - V_{series} \quad (3.3)$$

The voltage drop across the series resistance is easy to calculate through Ohm's law, which is the multiplication of the series resistance with the current:

$$V_{series} = I \times R_{series} = J \cdot Area \times R_{series} \quad (3.4)$$

As a result, the voltage across the solar cell itself becomes:

$$V_{effective} = V_{applied} - J \cdot Area \times R_{series} \quad (3.5)$$

Then, we could apply Equation 3.5 to the applied voltage, correcting for the series resistance, which allows us to look at current versus the effective voltage across the solar cell instead of the total applied voltage.

Correcting for series resistance is necessary, because when we calculate the photocurrent, we need to find the difference between dark current and light current at the same voltage. Before correcting for series resistance, we subtract the dark current from the light current at the same applied voltage. After learning more about the series resistance, we realized that at the same applied voltage, the effective voltage for the dark current is different from the effective voltage of the light current, because the contribution of series resistance due to the light current and dark current is different. Therefore, only after correcting for the series resistance, we are able to compare the light current and dark current at the equivalent effective voltage to extract the real photocurrent.

Figure 3-2 is the comparison between before and after correcting for series resistance for dark current, light current, and photocurrent. We observe that correcting

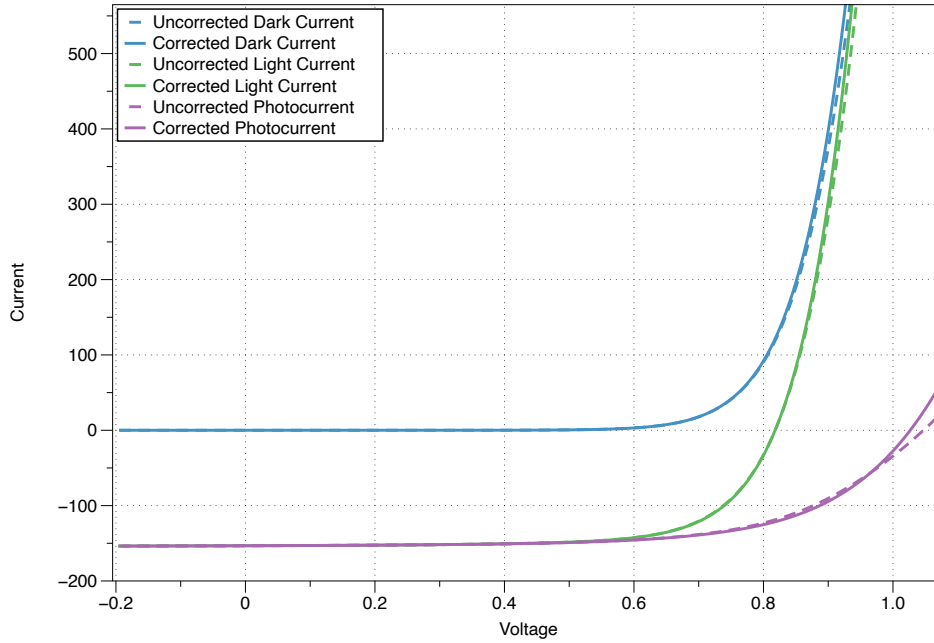


Figure 3-2: Before and after correcting for series resistance for dark current, light current and photocurrent: dashed lines represent current before correcting for series resistance and solid lines represent current after correcting for series resistance

Dark V	Dark I	Effective Dark V	Light V	Light I	Effective Light V
-0.190	-9.879e-10	-0.190	-0.192	-1.843e-4	-0.190
0.000	1.695e-10	0	0.000	-1.838e-4	0.000
0.200	3.531e-9	0.200	0.198	-1.828e-4	0.200
0.400	1.046e-7	0.400	0.398	-1.807e-4	0.400
0.600	3.698e-6	0.600	0.598	-1.710e-4	0.600
0.801	1.103e-4	0.800	0.799	-3.988e-5	0.800
1.000	1.417e-3	0.990	1.004	1.373e-3	0.990
1.200	5.288e-3	1.150	1.205	5.528e-3	1.150
1.400	1.120e-2	1.290	1.408	1.185e-2	1.290
1.600	1.868e-2	1.415	1.611	1.965e-2	1.415
1.810	2.767e-2	1.530	1.818	2.879e-2	1.530

Table 3.1: A typical example of correcting for the series resistance

for series resistance always shifts the current to the left. This makes sense because correcting for series resistance transforms the applied voltage into the smaller effective voltage. Also, the effect of correcting for series resistance is more significant at higher voltage, because higher voltage means larger current. This is reasonable because the voltage correction is equal to the voltage drop across the series resistance, which is

proportional to the current. Although the effect of correcting for series resistance may be not very significant at the voltage less than the compensation voltage, it provides us a better understanding of what is happening and makes our data more reliable. In addition, the effect of correcting for series resistance may be not very obvious when the current is small in general, as we have seen in Table 3.1. However, we still want to correct for series resistance. First, although the difference is small, it still exists, which provides better accuracy theoretically. Second, it allows us to analyze the current behavior in the solar cell itself by separating the influence of series resistance, which is critical for the development of our analytic model.

### 3.3 Adding Power Laws in the Photocurrent

Our goal is to modify our photocurrent fitting process by matching the true compensation voltage extracted from GPVDM with the compensation voltage extracted from the photocurrent. However, we found out that if we would like the compensation voltage extracted from the photocurrent to be equal to the true compensation voltage using the original fit equation, we need to manually change the fit range every time. The maximum fitting point depends on the shape of the photocurrent. It is not appropriate to manually change the fit point each time, because it will not give us a standard result. So, we started to think about the necessity of developing a new photocurrent fit equation that could give us a standard method of extracting the compensation voltage.

We observed an interesting phenomenon when we explored the original photocurrent fit. As shown in Figure 3-3, if we would like the original fit equation to match the shape of photocurrent at voltages near zero by increasing the fitting range, we could also get the match of lower voltages region for devices without traps. In other words, the shape of photocurrent for devices without traps is a sigmoid. However, for devices with traps, if we manually match the higher voltage part of the photocurrent, there is always a discrepancy in the low voltage region. We began to wonder why the shape of photocurrent for devices without traps have the perfect sigmoid shape,

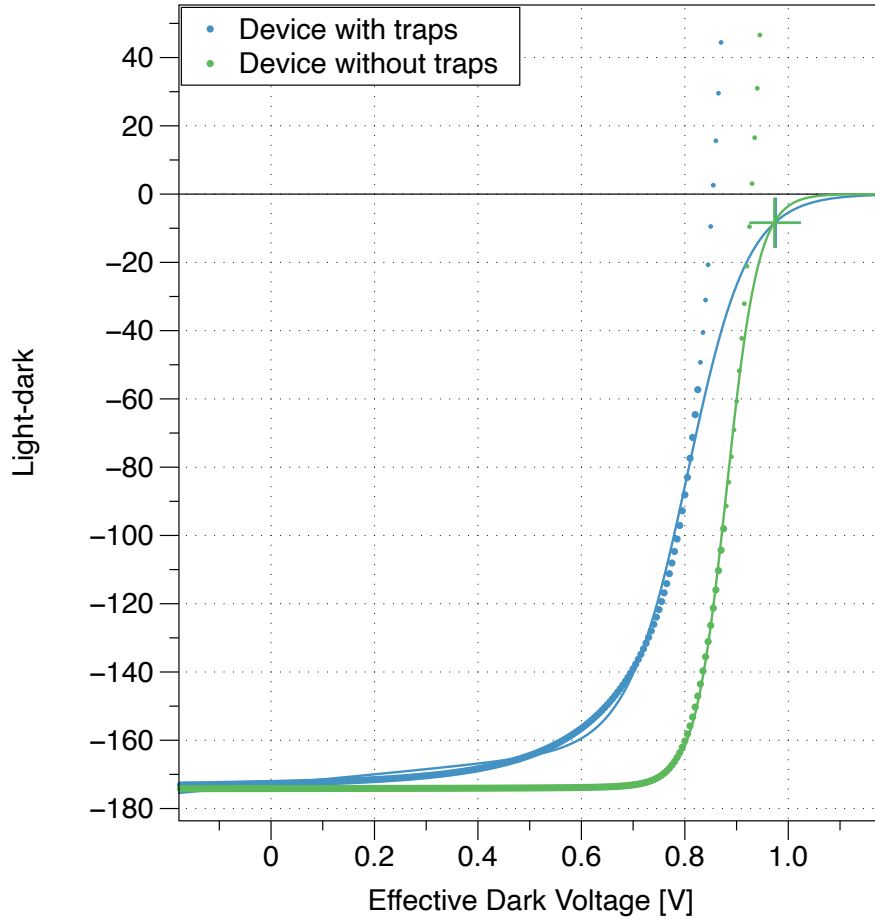


Figure 3-3: The old photocurrent fit for device with and without traps.

while the photocurrent for devices with traps do not.

We started to think about why traps could affect the shape of photocurrent. The discrepancy in photocurrent reminded us of the transport and recombination mechanisms in dark current. Previously, plotting the photocurrent did not yield a clear demonstration of the power law behavior, so we did not go into this direction. However, in looking at the difference between photocurrent calculated with traps and without traps, I realized this difference looked like it might follow a power law. Since the charge transport mechanism in dark current could also apply to photocurrent, we tried to add that physics into our photocurrent fit and it worked well.

Thus, we decided to add power law dependence to our photocurrent fit equation, because all the realistic devices have traps and the fundamental charge movement

mechanisms should be similar to the dark current. After trying many simulations and equations, we finally reach our latest equation for photocurrent as shown below:

$$-J\left(\frac{2}{1 + \frac{1}{1-jx-gx^h}} - \left(\frac{V}{V_0 + d}\right)^f\right) \quad (3.6)$$

“J” represents the maximum photocurrent, “j” is the coefficient for the ohmic shunt resistance, “g” and “h” are the coefficient and power for the shunting transport, “f” is the power for the recombination region, “V<sub>0</sub>” is the compensation voltage, and “d” accounts for the voltage offset of the compensation voltage.

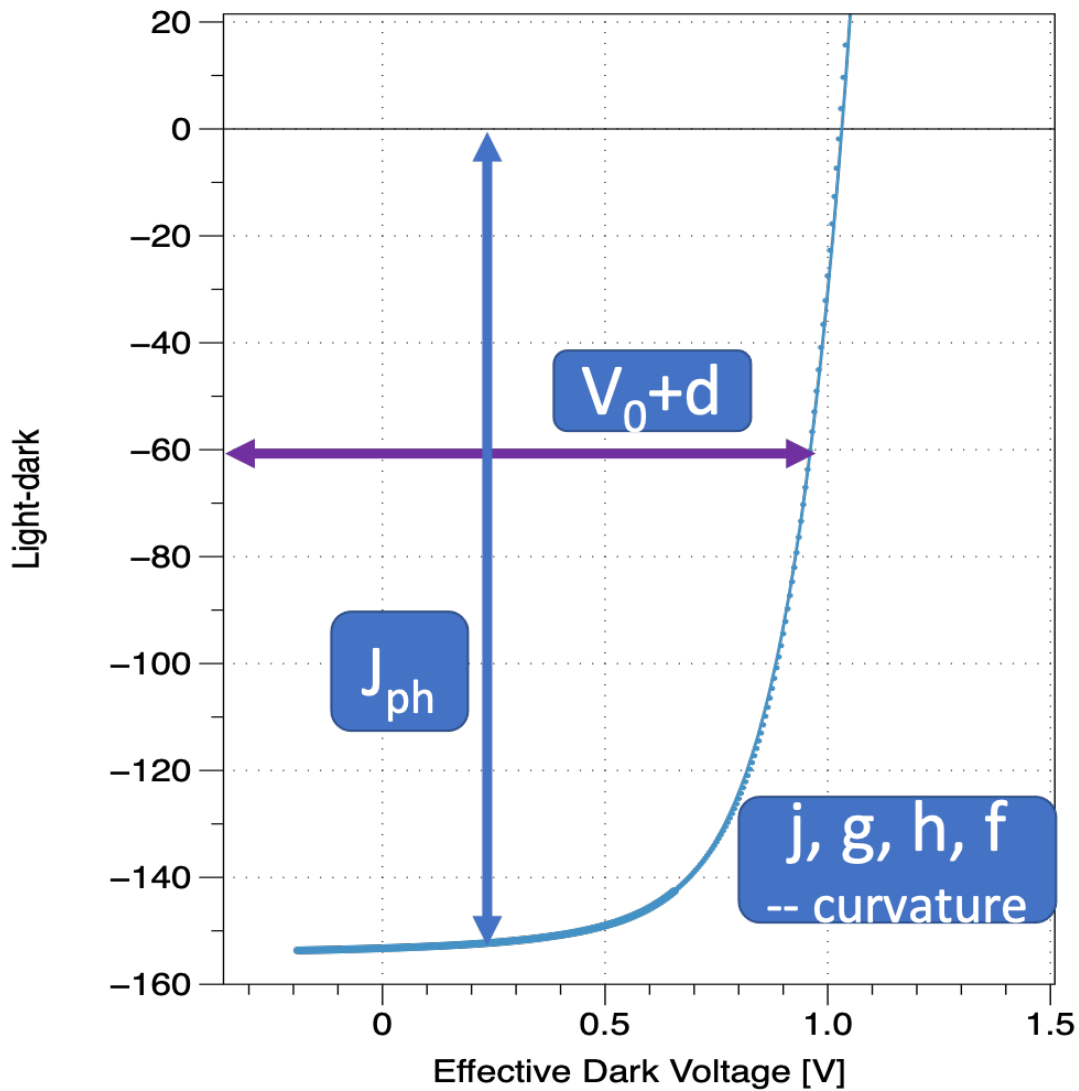


Figure 3-4: A typical new photocurrent fit with power laws

A typical fitting for the photocurrent using the new equation looks like Figure 3-4. We could easily extract “J”, “j”, “g”, “h”, “ $V_0 + d$ ”, and “f” from the fitting. The parameter “d” is believed to be a constant that depends on the temperature, so we need to set it to a value. Our previous default “d” was -0.08V based on our initial attempts. With the attempt to match compensation voltage from photocurrent with that from simulation, we recently adjusted our default “d” into -0.115. However, the value and meaning of “d” is still an open question and worth further discussion.

The compensation voltage extracted from the latest photocurrent equation is “ $V_0$ ” in the fitting parameter. Compared to the original photocurrent equation, one benefit of the new photocurrent equation is that it generates compensation voltage directly from the fitting parameters, instead of needing a separate relationship to calculate the compensation voltage. Another significant advantage is that the fitting can match the shape of a photocurrent not only in the low voltage region, but also at the region when the current is near zero, even if we only fit the low voltage region.

In addition, the compensation voltages extracted from the new fit equation agree with our fundamental assumption that the compensation voltages stay the same under different light intensities, as shown in Figure 3-5.

After adding the power law dependence to our new photocurrent equation, we now have the power law dependence in both dark current and photocurrent, which justifies our hypotheses on the physics of charge transport mechanism in solar cells.

### **3.4 Compensation Voltages Extracted from the New Fit Equation and the Interfacial Energy Difference**

From the physics of the recombination mechanism at the interface, we believe that there is a linear relationship between the compensation voltage and the energy difference between donor and acceptor. Although the statement above is still an assumption, we have suggestive experimental evidence. We would like to verify that

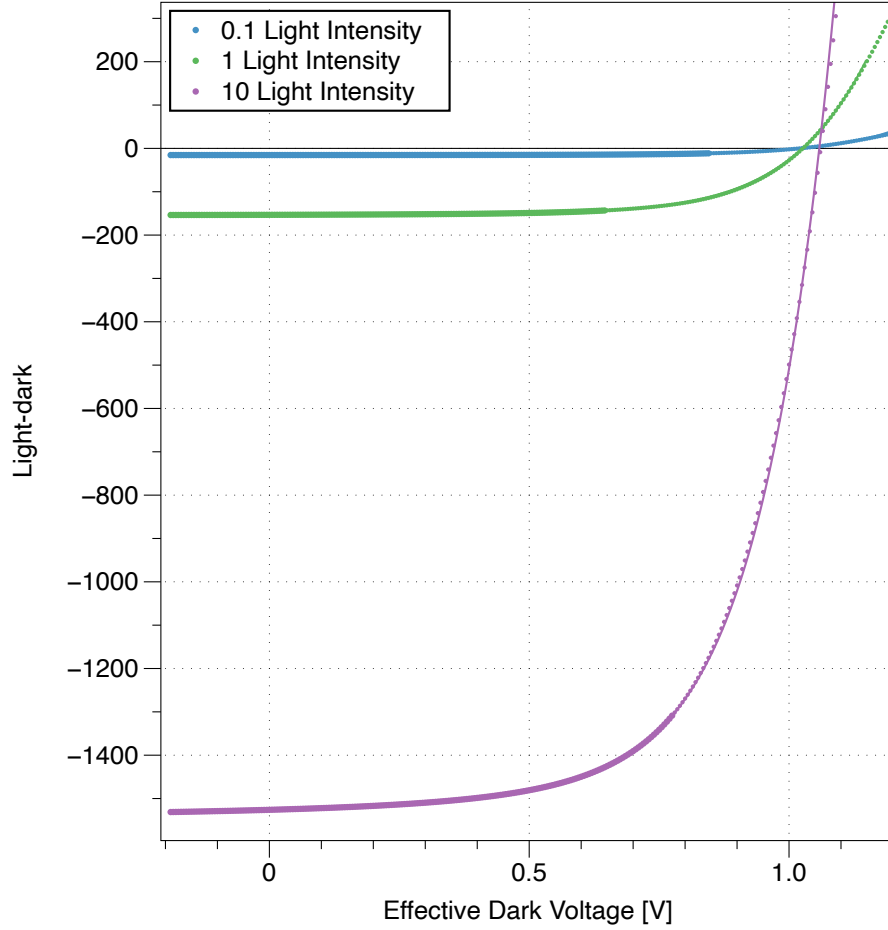


Figure 3-5: The photocurrent of three devices with 0.1 light intensity, 1 light intensity, and 10 light intensity. The corresponding compensation voltages extracted from the photocurrent fit are 1.20V, 1.21V, 1.21V

the relationship within simulation, which could validate our photocurrent model.

Energy Difference [eV]	$V_0$ from GPVDM [V]	$V_0$ from Photocurrent [V]
1.55	1.33	1.3173255
1.5	1.27	1.270126
1.45	1.19	1.2186895
1.4	1.17	1.1690931
1.35	1.09	1.1239441
1.3	1.07	1.0732513
1.25	0.99	1.0211536

Table 3.2: The extracted compensation voltages from GPVDM and photocurrent for devices with difference energy difference at the interface.

We simulated seven devices with interfacial energy difference as 1.55eV, 1.5eV,

1.45eV, 1.4eV, 1.35eV, 1.3eV, 1.25eV. The values of energy difference, compensation voltages from GPVDM, and compensation voltages from photocurrent fit is shown in Table 3.2. We would like the compensation voltages extracted from GPVDM to be equal to the compensation voltages from photocurrent. In Table 3.2, the compensation voltages from GPVDM are almost the same as the compensation voltages from photocurrent, as shown in figure 3-6.

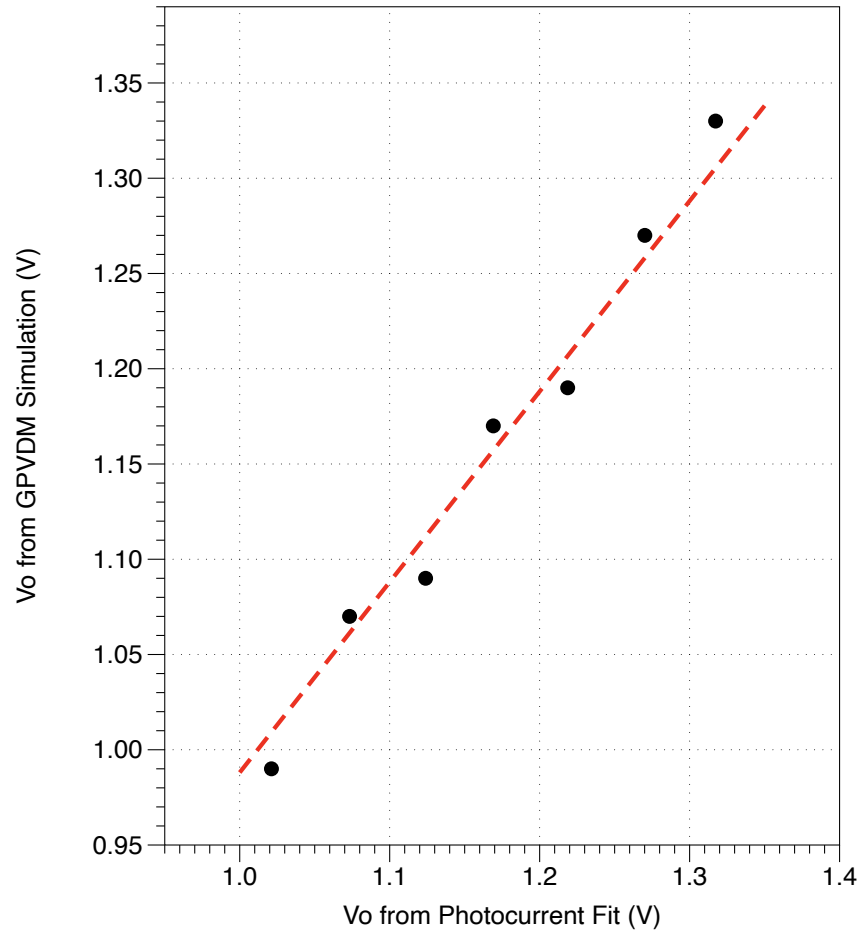


Figure 3-6: The plot of compensation voltages from photocurrent fit versus the compensation voltages from GPVDM. we fit a line with slope of one to the data, and got the fit equation as  $-0.01+x$ . The little offset is acceptable compared to the compensation voltages around 1.2V. The root mean square of the fit is  $-0.0119$ , which is also very small.

Figure 3-7 demonstrates the data and fit of photocurrent for three devices (the rest four devices have similar shapes and same trend). First, it shows that the fit of photocurrent follows the shape of the data points appropriately. Second, it presents

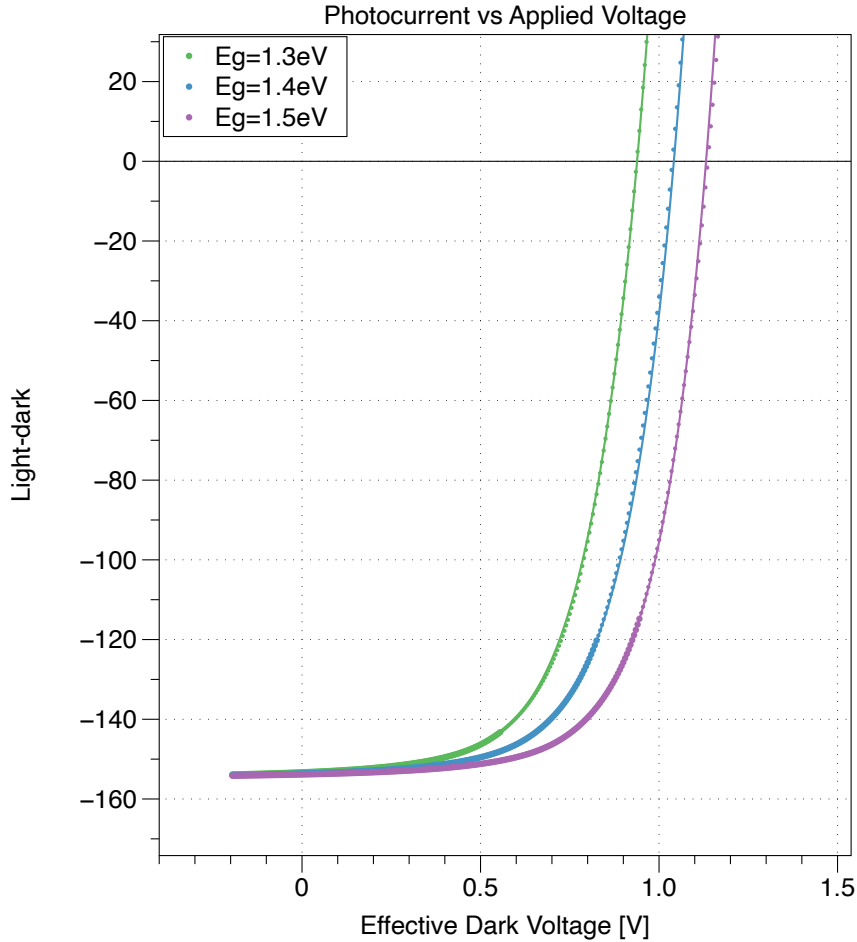


Figure 3-7: The photocurrent data and fit for three devices with energy difference 1.3 eV, 1.4 eV, and 1.5eV. The corresponding compensation voltages are 1.07V, 1.17V, and 1.27V.

the trend that the photocurrent shifts to the left as we have a smaller energy difference, corresponding with the decreasing compensation voltages, which is what we expect.

Figure 3-8 presents the relationship between the compensation voltage and the energy difference more directly. The dashed line is a fit to the compensation voltage versus energy difference, which shows the expected linear relationship between the compensation voltage and the energy difference with a slope of one. This means the compensation voltages could accurately reflect the energy difference at the interface, which is challenging to measure experimentally. However, there is still an offset between the compensation voltage and the energy difference. For example, in Figure 3-8, the offset is 0.21V. We need to acknowledge the exist of the offset, while when

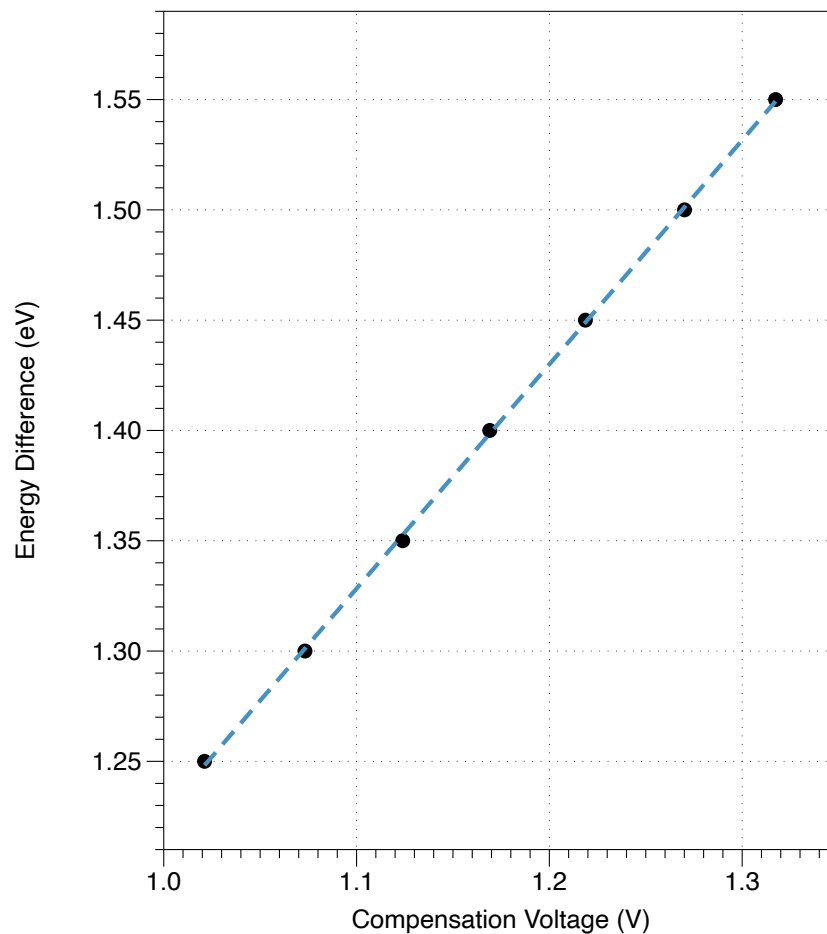


Figure 3-8: The relationship between compensation voltage and energy difference. The dashed line is fitted by software Datagraph with the function  $y = 0.21024 + 1.0164x$ . The root mean square is 0.0018443.

we analyze the change in interfacial energy difference, the offset is okay to be ignored. In general, we are content with the one to one relationship between compensation voltage and the energy difference at the interface.

In summary, the new photocurrent equation allows us to extract the compensation voltage from a simple fit, which we validate with simulation and can apply to experimental data.



# Chapter 4

## Discussion and Open Questions

Although the photocurrent equation works well for extracting compensation voltage from devices, there are still limitations and open questions on our fit equation and analytical model. In this chapter, I will discuss the shortcomings of the photocurrent equation, potential solutions, open questions, and our future plan in developing our analytical model for current in solar cells.

### 4.1 Extracted Compensation Voltages Depend on Trap Parameters

In the last chapter, I presented that the compensation voltage extracted from the photocurrent has a nice linear relationship with compensation voltage extracted from GPVDM. We reached the 1 : 1 relationship between the fit and GPVDM compensation voltages by setting the offset “d” as -0.115 V. However, what I have not mentioned is that the linear relationship only exists when all the other parameters of the solar cells are the same and only the energy difference changes. Specifically, we need to keep the trap parameters identical. If we change either trap depth or trap density, the linear relationship between the compensation voltage extracted from photocurrent and compensation voltage extracted from GPVDM will no longer exist.

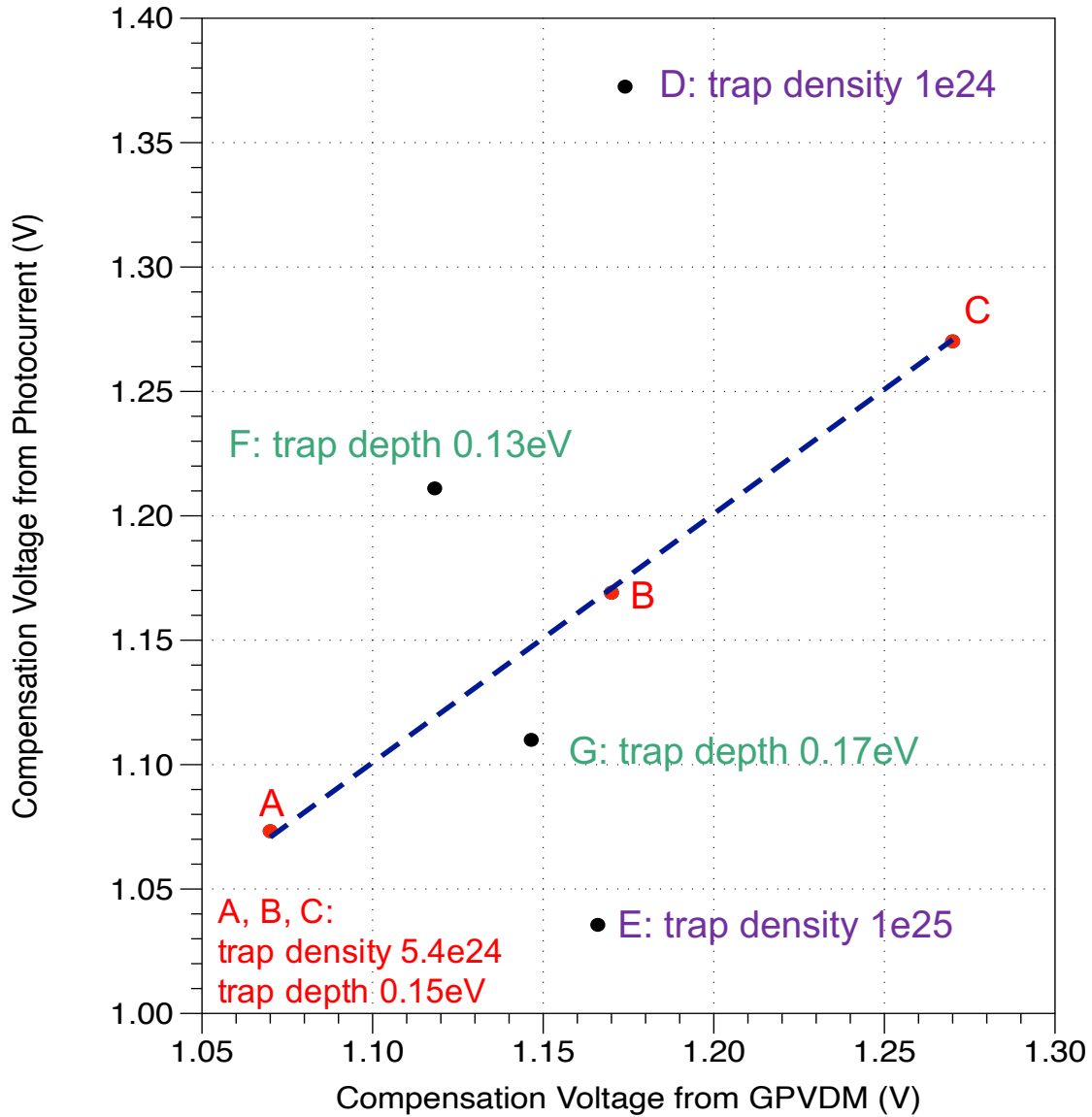


Figure 4-1: The plot of compensation voltages extracted from GPVDM versus compensation voltages extracted from photocurrent. Points A, B, C are devices with the same trap parameters: trap density  $5.4 \times 10^{24}$  and trap depth 0.15 eV. Points D, E, F, G are devices with different trap parameters. Device D has trap density  $1 \times 10^{24}$  and trap depth 0.15 eV; Device E has trap density  $1 \times 10^{25}$  and trap depth 0.15 eV; Device F has trap density  $5.4 \times 10^{24}$  and trap depth 0.13 eV; Device G has trap density  $5.4 \times 10^{24}$  and trap depth 0.17 eV. The dark blue line is fitted to points A, B, C with fit equation  $y = 0.00082346 + x$ . For the fit, the slope is set to be one, and the root mean square is 0.0021.

In Figure 4-1, the red points are from devices with the same trap parameters, where we could see the expected linear relationship between compensation voltage extracted from photocurrent and GPVDM. However, the other four black points, representing the devices with different trap parameters, deviate from the straight line.

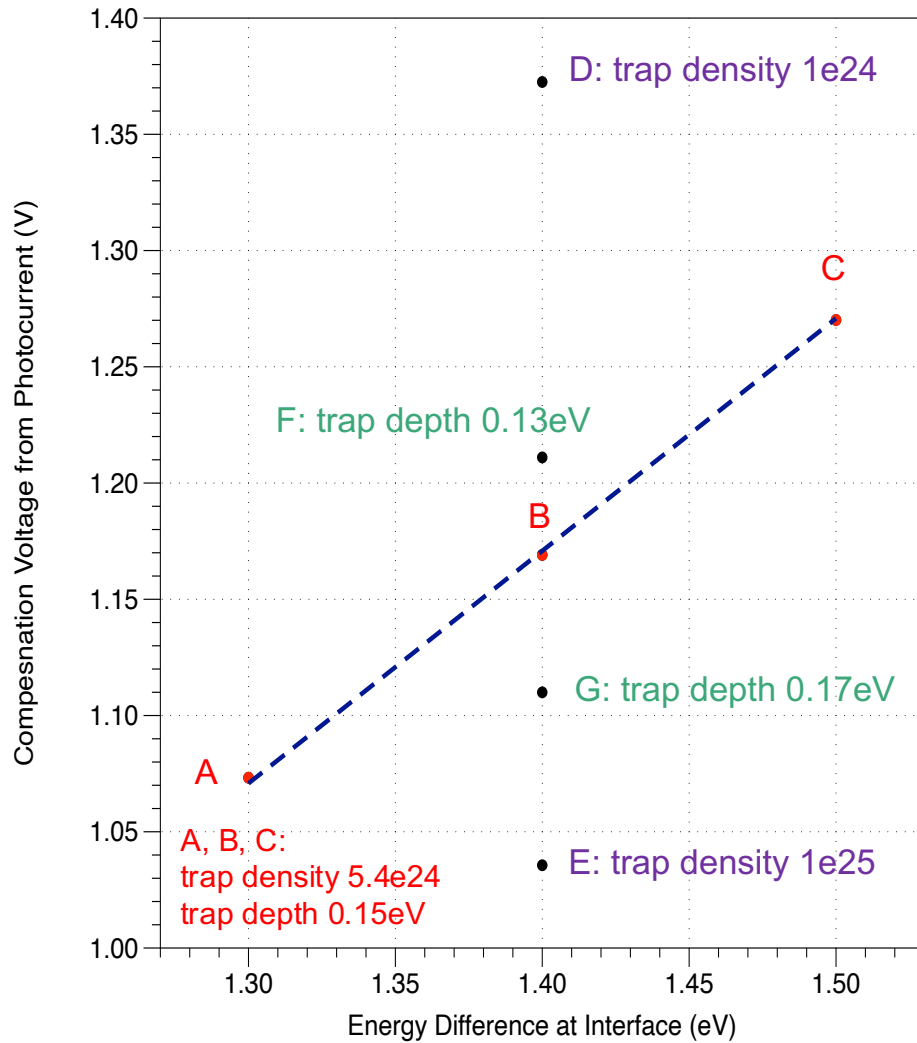


Figure 4-2: The relationship between the compensation voltage extracted from the photocurrent and the interfacial energy difference no longer holds when we change the trap parameters of the device. The dark blue line is fitted to points A, B, C with fit equation  $y = (-0.22918) + x$ . For the fit, the slope is set to be one, and the root mean square is 0.0021651.

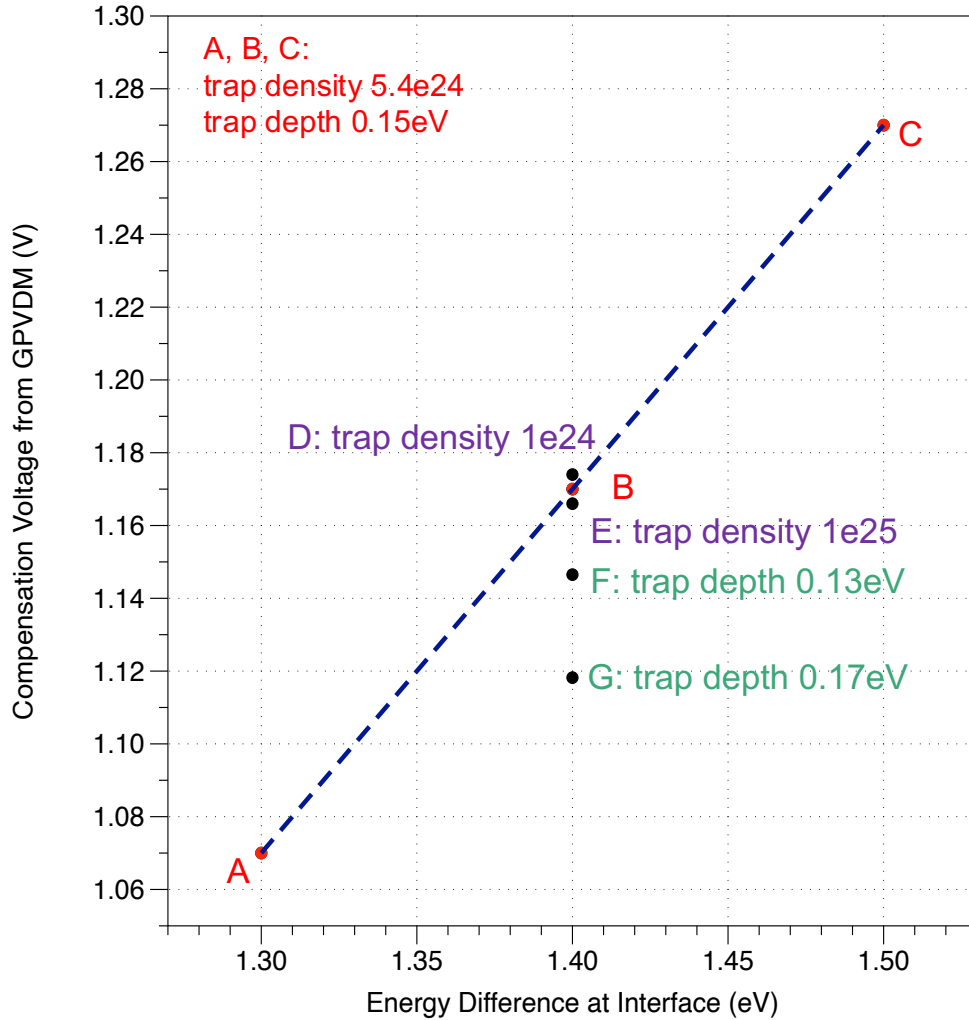


Figure 4-3: The relationship between the compensation voltage extracted from the GPVDM and the interfacial energy difference no longer holds when we change the trap parameters of the device. The dark blue line is fitted to points A, B, C with fit equation  $y = (-0.23) + x$ . For the fit, the slope is set to be one, and the root mean square is 0.

In addition to the relationship between compensation voltage extracted from photocurrent and GPVDM, the change of trap parameters also disturbs the linear relationship between compensation voltage and energy difference at the interface, as shown in Figure 4-2 and Figure 4-3. For both compensation voltages extracted from photocurrent versus energy difference and compensation voltages extracted from

GPVDM versus energy difference, the linear relationships only exist for devices with unchanged trap parameters. Figure 4-2 indicates that the Shunting and Transport Regions are not correctly accounted for by the fit equation. Figure 4-3 indicates that trap assisted recombination is not correctly accounted for by GPVDM. However, if we compare Figure 4-2 and Figure 4-3, we notice that the change in compensation voltages extracted from GPVDM is smaller than that in compensation voltages extracted from photocurrent. This observation suggests that the compensation voltages extracted from GPVDM have less dependency on traps compared to compensation voltages from photocurrent and that we need to better understand what this difference tells us about the two techniques.

To understand why extracted compensation voltages from the photocurrent fit are impacted by traps, we need to consider what the offset “d” in the photocurrent equation means. One of our hypotheses is that “d” may be analogous to the ideality factor in the typically used exponential model, which contains important information about the recombination and transport in solar cells and depends on traps [28]. Therefore, when the traps are different, the value of “d” will also change. Recall that what we extract from the photocurrent equation is “ $V_0 + d$ ”. However, we determined “d” with one set of electrical parameters and kept “d” fixed as we changed the traps. In this way, it is possible that the extracted compensation voltages are changing because we fail to take the change of “d” into account, while the actual compensation voltages may remain constant. We need to further study d’s dependence on traps and modify our fit equation accordingly.

Furthermore, the ambiguity on the meaning of “d” may be related to our assumption about the photocurrent. As discussed in Section 1.2.4, the flat band voltage is equal to the compensation voltage when all the current is drift current. We make the assumption that all the current is drift current in our simulation, and our extracted compensation voltages seem to suggest this assumption works. However, it is also likely that we did not include the full picture of the current, and “d” is acting as a parameter related to the non-drift current. In this way, we should not be surprised by “d” acting as an offset. This could also explain the discrepancy between compen-

sation voltages extracted from photocurrent and GPVDM, because the voltage we extracted from the GPVDM is the flat band voltage, while there will be the offset between flat band voltage and compensation voltage with non-drift current.

It is reasonable that the change in traps will indeed change the compensation voltage, because traps are critical for recombination inside the solar cells. The compensation voltage could be affected by both the interfacial energy difference and the trap characteristics. Thus, the change in compensation voltage based on traps may be expected.

In summary, our future work includes finding out the true meaning of offset “d” in the photocurrent fit, specifically figuring out whether “d” is a constant or depends on traps. Then, we will use the improved fit equation to keep investigating the expected numeric relationship in our analytical model, such as the relationship between compensation voltages and the interfacial energy difference.

## 4.2 Development of Dark Current Model

The understanding of power laws in dark current is why we choose to use power laws for the photocurrent. While the dark current modeling is not the subject of this thesis, the model of dark current is critical for understanding more about the photocurrent. While we developed the photocurrent fit equation, our lab continued to build the model of dark current. For example, we still lack physical theories for the recombination term of dark current, and one of my labmates is working on deriving an analytical expression for that. In addition, we are reconsidering if our schematic of the solar cells in Figure 1-22 is correct. Specifically, it is unclear whether our device shows evidence for the space-charge limited conduction without traps. After our dark current model is updated, the photocurrent model will be modified correspondingly. The good news is that our research on photocurrent now seems to capture the essential ideas, and further modifications may happen on a detailed level. Importantly, working with GPVDM has given us a process to evaluate changes to the photocurrent model, which we could apply to improve future photocurrent models.

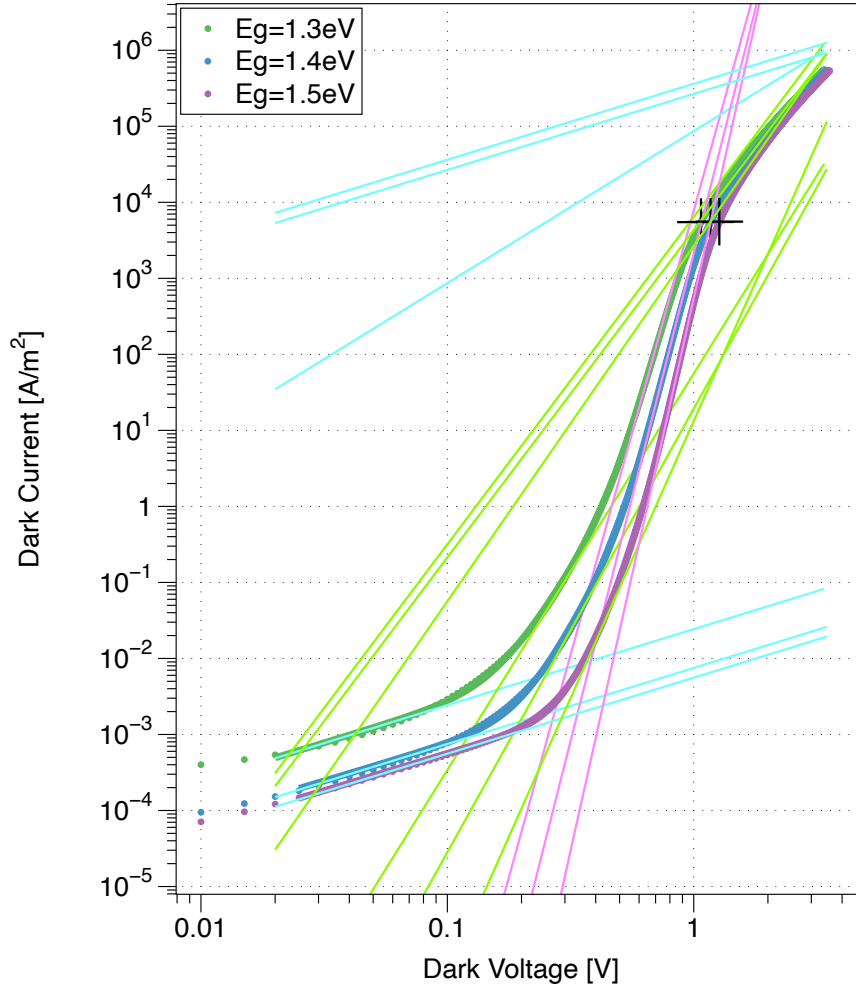


Figure 4-4: Typical positions of compensation voltages in dark current fit. The compensation voltages are marked by the black + signs. Note that they are located where the pink (recombination) and green (transport) lines intersect.

The photocurrent model also can help us understand the voltage distribution in dark current. We hypothesize that the compensation voltage should be around the transition position of the recombination region and the transport region in dark current, because the recombination will happen when the band approaches flat, and when the band is roughly flat the device is entering the transport regime. The typical position of compensation voltage in a dark current fit is shown in Figure 4-4. The pink lines represent the recombination term, and the light green lines above them represent the transport term. After extracting the values of compensation voltages from the photocurrent fit, we mark the compensation voltages on the dark IV curve

using the black “+” signs. The positions of compensation voltage in Figure 4-4 are roughly the same as our expectation.

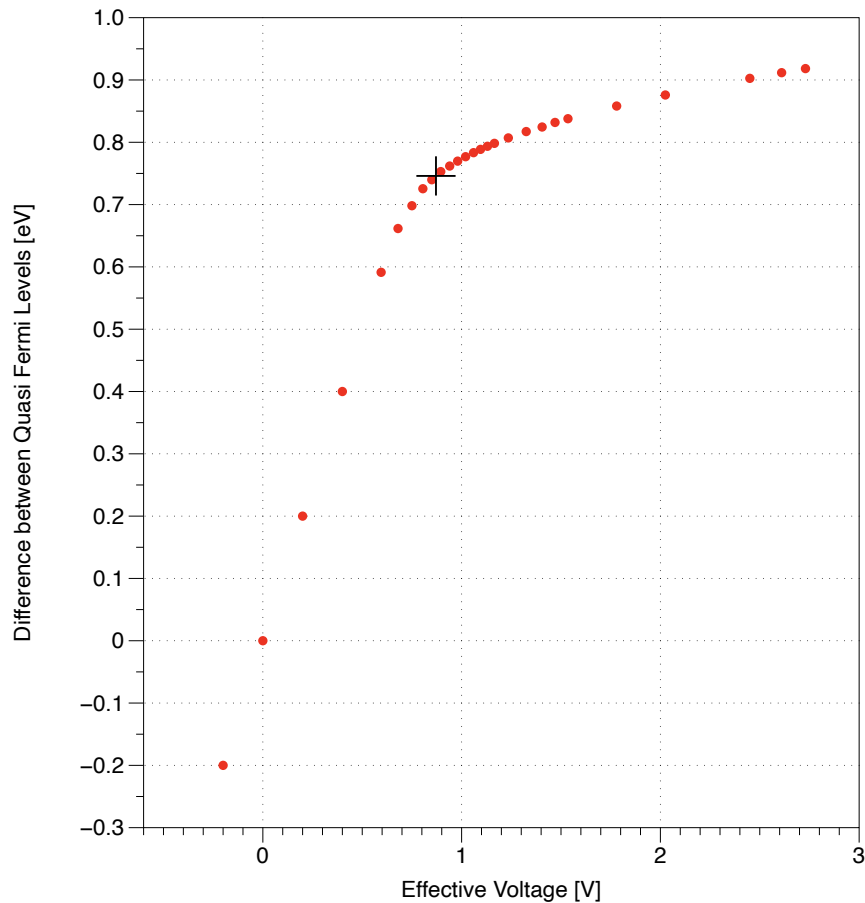


Figure 4-5: The plot of the difference in quasi Fermi levels at the interface versus the effective voltage. The quasi Fermi levels difference is calculated by the electron quasi Fermi level minus the hole quasi Fermi level as determined by GPVDM. The black + sign marks the position of the compensation voltage.

We need to consider the voltage distribution within solar cells to correctly add their contribution to the total current, which we have mentioned in Section 1.3.4. When we correct for series resistance, we isolate the solar cell from the rest of the device. Similarly, we could isolate the voltage drop at the interface from the other parts of the solar cell to investigate voltage distribution inside solar cells. We believe that almost all the voltage is dropped at the interface before the compensation voltage, and the voltage dropped at the interface stays roughly constant after the compensation voltage. The energy drop at the interface is equal to the difference in quasi Fermi

level of holes and electrons at the interface, so we plot the difference of quasi Fermi levels to test our assumption, as shown in Figure 4-5. The general trend in energy difference at the interface is the same as our expectation, except that the turning regime needs to curve to avoid an abrupt transition. While our hypothesis on voltage distribution is still a work in progress, we have to acknowledge that the voltage distribution approximation we use right now is linear for all the voltages (without the roughly flat part after the compensation voltage), for devices like Figure 4-4, which may not be physical. The change of the voltage distribution inside solar cells may adjust the fit slightly but not change the fit significantly.

Our ultimate goal is to unify the physics in dark current and photocurrent, and I will talk more about the unification in the next section.

### 4.3 Unifying Powers in both Photocurrent and Dark Current

Before I began to work on this thesis, we focused on analyzing the charge transport mechanism in dark current. At that time, our model had power law dependence in only the fit equation of the dark current, not in photocurrent.

After studying more about the photocurrent, we realized that the power laws also apply to the photocurrent. The only difference is that we need to take the constantly generated photocurrent into account. Then, the physics of dark current is also valid in the photocurrent.

We expect the fitting powers in photocurrent to be identical with those in dark current, because they have the same physical meanings. For example, we expect the fitting parameter that describes the recombination term in dark current (M) to be identical with the corresponding parameter in photocurrent (F). However, we currently fit dark current and photocurrent separately, and the fitting parameters from dark current and photocurrent are not identical. From the existing simulation work, we observed that when the power representing recombination in photocurrent (F)

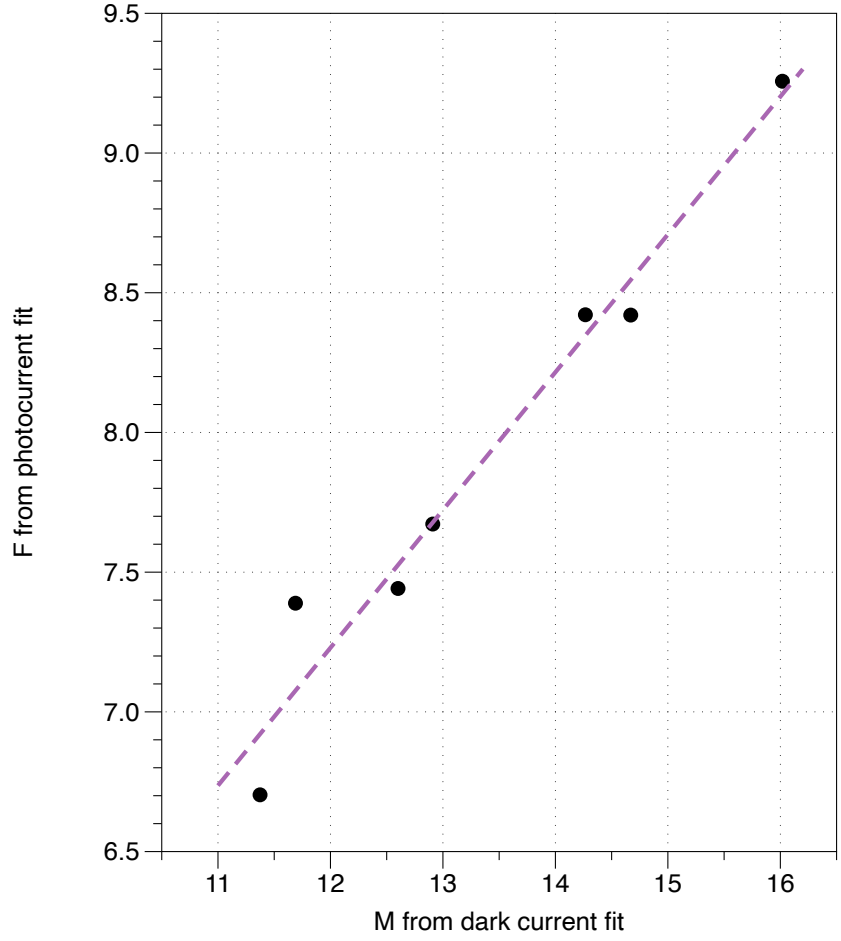


Figure 4-6: The plot of M from dark current fit versus F from the photocurrent fit. Both M and F represent the fitting parameters of the recombination term of the solar cells.

Eg	Vo from photocurrent	Vo from simulation	M	F
1.55	1.32	1.33	16.018568	9.256949
1.5	1.27	1.27	14.669871	8.4200714
1.45	1.22	1.19	14.266613	8.4212039
1.4	1.17	1.17	12.90954	7.6722126
1.35	1.12	1.09	12.600708	7.4415955
1.3	1.07	1.07	11.68903	7.3888743
1.25	1.02	0.99	11.374013	6.703083

Table 4.1: The table of energy difference, compensation voltage from photocurrent and simulation, and the fitting parameters for recombination term in dark current (M) and photocurrent (F).

increases, the power representing recombination in dark current ( $M$ ) also increases, as shown in Figure 4-6, while they are not identical to each other. Table 4.1 shows the values of these fitting parameters.

The discrepancy between the fit powers in photocurrent and dark current indicates that our fit equation needs to be improved. It is likely that we miss a term in the fit equation or make errors when adding different contributions. It could also be that we are not using the correct offset “d” with trap dependency. Another potential problem may be that the parameters we extracted have slightly different physical meanings compared to what we expect, so the powers are not meant to be identical. However, that is not what we want. If the last situation is true, we need to keep improving our fit equation by investigating the extra relationships between the fit parameters and the physical values.

In the future, we also plan to write programs in python to fit the photocurrent and dark current simultaneously to reach the same or correlated fitting parameters. One of my labmates is currently working on this project.

## 4.4 Assess the analytical model with experimental data

There are multiple open questions on the relationship between the analytical model and the experimental data. One of the most important questions is that what can the simulation tell us about the experiment?

First, the simulation could reproduce several expected characteristics in the experiments, such as the fact that compensation voltage is constant under different light intensities and the linear relationship between the energy difference and the compensation voltage. Those recurring relationships in simulation verify our model and make us more confident about our hypotheses.

We developed our analytical model based on simulation and would like to validate our model with the experimental data. For example, we plan to re-extract the

compensation voltage from the previous experiments. However, there are many challenges when we try to apply the new fit equation to the experimental data. One of the problems is that we do not know the series resistance in the experimental data, because we do not measure it. As a result, we cannot correct for series resistance.

Fit Parameters	Series Resistance 10	Series Resistance 50	Series Resistance 100
$J_{ph}$	1.9235654	1.9216051	1.9224669
$V_0$	1.2769087	1.2757532	1.2763138
d	-0.08	-0.08	-0.08
F	7.8230032	7.6380142	7.7314527
H	1.6568701	1.2103406	1.404012

Table 4.2: Fitting the same experimental data with series resistance equal to 10  $\Omega$ , 50  $\Omega$ , and 100  $\Omega$ .

I have tried correcting for several possible series resistance values in a set of experimental data. As shown in table 4.2, I corrected for 10  $\Omega$ , 50  $\Omega$ , and 100  $\Omega$  series resistance as tests. The result is that the effect of correcting for series resistance is almost negligible. It is understandable, because the experimental current is too low, and the experimental current does not get to high enough voltage. On one side, this is good, because we do not know how to correct for series resistance, and this suggests that we don't need it. However, we still don't know how to correct for series resistance if we need it.

We believe that we can estimate a maximum value for the series resistance by increasing the series resistance until the data points began to jump abnormally. And the series resistance of the device must be smaller than the series resistance that makes the data collapse. This works with the simulated data, but we are not confident if it will work on experimental data.

Another idea is to include series resistance in our analytical model. Currently, we first correct for series resistance, and then apply our model without series resistance to the data. If we figure out a way to include the effect of series resistance in our model, we can apply the new model to experimental data directly, without the need of knowing its series resistance. The correction of series resistance in simulation has already helped us to better understand the effect of series resistance, and we are

working on applying our better understanding of the series resistance to obtain an analytical model with the correct effect of series resistance.

Last but not least, we always would like to use simulation to reproduce the experimental data. We have tried to use reasonable ranges for each electrical parameter in simulation, which is our first step towards approaching realistic parameters. Using GPVDM to match the experimental data is the next step, so that we can be sure that our work on modeling the photocurrent is consistent with our actual devices. The electrical parameters I used were based on our best guesses at the time and convenience. I selected a symmetric device instead of the more realistic asymmetric device. In addition, I started my set of simulations before we matched the simulation parameters with the experimental data. While many values are similar, we need to verify our results with matched parameters, which are included in Appendix A for the one experimental device that we have modelled in GPVDM so far.

## 4.5 Summary and Future Plans

In this thesis, I discussed how we developed our analytical model for photocurrent in solar cells and were able to extract compensation voltage from the model.

We began with a description of our previous work on charge transport mechanisms in the dark current of solar cells. We divided the dark current into five regions with different voltage dependencies and analyzed their physics: Shunt Resistance, Shunting, Recombination, Transport, and Series Resistance. We used power-law dependencies to analyze the physics for each charge transport mechanism. Among them, the recombination at the interface is related to the energy difference between the donor and acceptor layer, and we expect to find the compensation voltage at the transition point between recombination and transport regions. In addition, the space charge limited current with traps in the transport region reflects the distribution of traps in the solar cells. We created an analytic equation to describe all the contributions for dark current and studied the fit parameters. Our dark current model is unique, because it incorporates the actual physics of transport in disordered materials into

an analytical equation.

After getting a comprehensive understanding of dark current, we started to think about whether the physics of dark current could also be applied to the photocurrent. Our goal is to extend our model to include photocurrent and find a method for extracting compensation voltage directly from the photocurrent. Simulation allows us to control many electrical parameters, and can be used to calculate a number of different properties of the device.

With the band diagram and potential provided by the simulation software, GPVDM, we are able to determine the true compensation voltage of a solar cell. After trying several different photocurrent fit equations, we realized that power law dependence should be added to the photocurrent. Including the power laws in the photocurrent model is a huge improvement from where we began, matching the shape of typical photocurrent and unifying the physics of dark current and photocurrent. Comparing the compensation voltages extracted from the GPVDM and the compensation voltages extracted from photocurrent, we established a new photocurrent equation.

From the new photocurrent fit equation, we got the expected relationship between compensation voltage from GPVDM and photocurrent as well as between energy difference and compensation voltage for the devices with the same trap parameters. Our next step is to investigate the trap dependencies of the compensation voltages and use that to improve our photocurrent fit equation.

Moreover, we plan to unify the simulation with experiments. Specifically, we are working on refitting our previous experimental data to extract compensation voltage and validate the expected numerical relationship between compensation voltage and energy difference.

In addition to my work on photocurrent, my lab mates are working on broader topics related to our analytical model of current in solar cells. Hadley O'Malia is working on an equation for the recombination term to form a solid theoretical background of our hypothesis that the steep rise in dark current is a power law that depends on the energy difference at the interface. Ji-Won Ham is working on simulating single layer devices to further investigate the effect of space charge limited current in the

presence of traps. Christina McGahan is matching experimental data with GPVDM to find more realistic electric parameters for the simulations and the corresponding fit parameters of experiments. Ayla Osgood is coding the fitting process in python, so that we could fit photocurrent and dark current simultaneously, setting equivalent powers to be the same. All the work above will help us better understand the physics of current in solar cells as a whole and improve our analytical model.

While this thesis greatly improved our understanding of photocurrent and demonstrated an analytical model, the most important contribution is likely the process that we used. By figuring out how to use GPVDM to simulate the solar cells, and understanding its limitations, we were able to develop a dataset to compare the “true” compensation voltage with one extracted by the equation for photocurrent. With the method of evaluating a fit equation, we could keep developing our analytical model. There are still many open questions, and I am sure that my work is going to be improved by someone else, as is the case throughout the development of science, to reach a better analytical model for current in solar cells.

I am looking forward to that—a better version of our future.



# Appendix A

## Realistic Electric Parameters

Names	Donor Layer 1	Donor Layer 2
DOS Distribution	exponential	exponential
Electron Trap Density	5.4e24	5.4e24
Hole Trap Density	5.4e24	5.4e24
Electron Tail Slope	0.15	0.15
Hole Tail Slope	0.15	0.15
Electron Mobility	1e-6	2e-6
Hole Mobility	1e-6	2e-6
Relative Permittivity	3.0	3.0
Number of Traps	5	5
Free Electron to Trapped Electron	1e-21	1e-21
Trapped Electron to Free Hole	1e-21	1e-21
Trapped Hole to Free Electron	1e-21	1e-21
Free Hole to Trapped Hole	1e-21	1e-21
Effective Density of Free Electron	5e25	8e24
Effective Density of Free Hole	5e25	8e24
$\Xi$	3.25	3.25
$E_g$	2.35	2.35
Free to Free Recombination Rate	0	0

Table A.1: The comparison between the simulation electric parameters that I use and the more realistic parameters our group recently found. Donor Layer 1 shows the parameters I use in the simulation for an ideal symmetrical device. Donor Layer 2 is based on matching the simulation data with the experimental data, which provides more realistic parameters.

Table [A.1](#), [A.2](#), [A.3](#) present the comparisons between the electric parameters for my simulation and our group's latest simulation based on matching experimental data

Names	Acceptor Layer 1	Acceptor Layer 2
DOS Distribution	exponential	exponential
Electron Trap Density	5.4e24	5.4e24
Hole Trap Density	5.4e24	5.4e24
Electron Tail Slope	0.15	0.15
Hole Tail Slope	0.15	0.15
Electron Mobility	1e-6	2e-6
Hole Mobility	1e-6	2e-6
Relative Permittivity	3.0	3.0
Number of Traps	5	5
Free Electron to Trapped Electron	1e-21	1e-21
Trapped Electron to Free Hole	1e-21	1e-21
Trapped Hole to Free Electron	1e-21	1e-21
Free Hole to Trapped Hole	1e-21	1e-21
Effective Density of Free Electron	5e25	8e24
Effective Density of Free Hole	5e25	8e24
$\chi_i$	4.2	4.2
$E_g$	2.35	2
Free to Free Recombination Rate	0	0

Table A.2: The comparison between the simulation electric parameters that I use and the more realistic parameters in acceptor layer.

for the donor layer, acceptor layer and middle layer. The parameters I use for donor and acceptor layers do not change a lot from the more realistic parameters. However, the difference between the parameters I use for the middle layer and that for realistic device is more obvious, as shown in Table A.3.

One of our future plan is to test our photocurrent model in the devices with the more realistic parameters. I believe that the future simulation with more realistic electric parameters could build better conclusions and theories on the top of my current study.

We also need to acknowledge that the more realistic parameters could be updated in the future if we figure out a better way to match the simulation with experimental work.

Names	Middle Layer 1	Middle Layer 2
DOS Distribution	exponential	exponential
Electron Trap Density	5.4e24	9e23
Hole Trap Density	5.4e24	9e23
Electron Tail Slope	0.15	0.2
Hole Tail Slope	0.15	0.2
Electron Mobility	1e-6	2e-6
Hole Mobility	1e-6	2e-6
Relative Permittivity	3.0	3.0
Number of Traps	5	5
Free Electron to Trapped Electron	1e-21	6e-19
Trapped Electron to Free Hole	1e-21	1.2e-22
Trapped Hole to Free Electron	1e-21	6e-21
Free Hole to Trapped Hole	1e-21	6e-19
Effective Density of Free Electron	5e25	8e24
Effective Density of Free Hole	5e25	8e24
Xi	4.2	4.2
Eg	1.4	1.4
Free to Free Recombination Rate	0	0

Table A.3: The comparison between the simulation electric parameters that I use and the more realistic parameters in middle layer.



# Appendix B

## Full Dark Current Equation

In Chapter 1, I introduced the equation of each contribution of dark current separately. In this appendix, I will write down the full dark current equation we have right now.

First, Let's rename and rewrite the current of each contribution.

$$J_s = \frac{V}{R_s A} \quad (\text{B.1})$$

$$J_{sh} = \frac{V}{R_{sh} A} \quad (\text{B.2})$$

$$J_{SH} = bV^B \quad (\text{B.3})$$

$$J_R = mV^M \quad (\text{B.4})$$

$$J_T = nV^N \quad (\text{B.5})$$

$J_s$  represents the current due to series resistance,  $J_{sh}$  represents the current due to shunt resistance,  $J_{SH}$  represents the current due to Shunting,  $J_R$  represents the current due to Recombination, and  $J_T$  represents the current due to Transport.

For the two ohmic contributions (series resistance and shunt resistance), the current is equal to the voltage divided by the resistance. We also need to divide by the area of the solar cell (A), because we use current density to represent the contribution. For the other three contributions (Shunting, Recombination, Transport), we add corresponding constants (b, m, n) to describe the proportionality between the current contribution and voltage dependence.

Then, the next step is to add these current together follow the circuit diagram. Therefore, we reach the total current as:

$$J_{dark} = \frac{1}{\frac{1}{J_s} + \frac{1}{J_{sh} + \frac{1}{\frac{1}{J_T + J_R + J_{SH}}}}} \quad (\text{B.6})$$

# Bibliography

- [1] Pieter Kuiper. Comparison of the electronic band structures of metals, semiconductors and insulators, 6 June 2007.
- [2] Ben G. Streetman. *Solid State Electronic Devices*. Prentice-Hall.
- [3] Ji-Won Ham. Investigating transport limits through traps for higher solar cell efficiency. *Mount Holyoke College Physics Department Summer Poster Session*, 2020.
- [4] Santiago Silvestre. Chapter 7 - strategies for fault detection and diagnosis of pv systems. In Imene Yahyaoui, editor, *Advances in Renewable Energies and Power Technologies*, pages 231–255. Elsevier, 2018.
- [5] Swati Chaudhary, Varsha Yadav, Chandra Mohan Singh Negi, and Saral K Gupta. Charge transport and impedance analysis of solution-processed perovskite-based device. *Micro & Nano Letters*, 15(3):136–139, 2020.
- [6] A Wallace Copeland, Otis D Black, and A B Garrett. The photovoltaic effect. page 50.
- [7] Jenny A. Nelson. *The Physics Of Solar Cells*. World Scientific Publishing Company. Google-Books-ID: 4Ok7DQAAQBAJ.
- [8] Albert Einstein. Über einen die Erzeugung und Verwandlung des Lichtes betreffenden heuristischen Gesichtspunkt. (German) [on a heuristic point of view about the creatidn and conversion of light]. *Annalen der Physik*, 17(6):132–148, 1905.

- [9] Ashley Cavanagh. *Development of Atomic Force Microscope Techniques for Extracting Work Function and Density of States*. PhD thesis, Mount Holyoke College, 2019.
- [10] Uli Würfel Peter Würfel. *Physics of Solar Cells: From Basic Principles to Advanced Concepts*. WILEY-VCH.
- [11] Andreas Petersen, Thomas Kirchartz, and Thomas A Wagner. Charge extraction and photocurrent in organic bulk heterojunction solar cells. *Physical Review B*, 85(4):045208, 2012.
- [12] Syed A. Moiz, Iqbal. A. Khan, Waheed A. Younis, and Khasan S. Karimov. Space charge-limited current model for polymers. In Faris Yilmaz, editor, *Conducting Polymers*, chapter 5. IntechOpen, Rijeka, 2016.
- [13] Kathleen T. Smith. *Modelling Current-Voltage Characteristics in Organic Photovoltaics*. PhD thesis, Mount Holyoke College, 2018.
- [14] Manijeh Razeghi. *Fundamentals of solid state engineering*, volume 23. Springer, 2009.
- [15] N. C. Giebink, G. P. Wiederrecht, M. R. Wasielewski, and S. R. Forrest. Ideal diode equation for organic heterojunctions. i. derivation and application. *Phys. Rev. B*, 82:155305, Oct 2010.
- [16] A. Foertig, J. Rauh, V. Dyakonov, and C. Deibel. Shockley equation parameters of p3ht:pcbm solar cells determined by transient techniques. *Phys. Rev. B*, 86:115302, Sep 2012.
- [17] Mohamed B.H. Rhouma, Adel Gastli, Lazhar Ben Brahim, Farid Touati, and Mohieddine Benammar. A simple method for extracting the parameters of the pv cell single-diode model. *Renewable Energy*, 113:885–894, 2017.
- [18] Luis Chuquimarca, Ximena Acaro, Alfonso Gunsha, Luis Villamagua, and David Sánchez. Two-diode model parameter evaluation from dark characteristics of

- back-contact back-junction solar cells. In *The 2018 International Conference on Digital Science*, pages 200–207. Springer, 2018.
- [19] Brett J Hallam, Phill G Hamer, Ruy S Bonilla, Stuart R Wenham, and Peter R Wilshaw. Method of extracting solar cell parameters from derivatives of dark i–v curves. *IEEE Journal of Photovoltaics*, 7(5):1304–1312, 2017.
- [20] Amit Singh Rajput, Jian Wei Ho, Yin Zhang, Srinath Nalluri, and Armin G Aberle. Quantitative estimation of electrical performance parameters of individual solar cells in silicon photovoltaic modules using electroluminescence imaging. *Solar Energy*, 173:201–208, 2018.
- [21] Antonino Laudani, Francesco Riganti Fulginei, Fernando De Castro, and Alessandro Salvini. Irradiance intensity dependence of the lumped parameters of the three-diodes model for organic solar cells. *Solar Energy*, 163:526–536, 2018.
- [22] Roland Dietmueller, Helmut Nesswetter, Sebastian J Schoell, Ian D Sharp, and Martin Stutzmann. Band alignment at organic–inorganic heterojunctions between p3ht and n-type 6 h-sic. *ACS applied materials & interfaces*, 3(11):4286–4291, 2011.
- [23] Dominique J Wehenkel, L Jan Anton Koster, Martijn M Wienk, and René AJ Janssen. Influence of injected charge carriers on photocurrents in polymer solar cells. *Physical Review B*, 85(12):125203, 2012.
- [24] RA Street, KW Song, and S Cowan. Influence of series resistance on the photocurrent analysis of organic solar cells. *Organic Electronics*, 12(2):244–248, 2011.
- [25] Katherine Aidala. Dark iv model. Documentation, Mount Holyoke College, 2021.
- [26] Roderick C. I. MacKenzie, Thomas Kirchartz, George F. A. Dibb, and Jenny Nelson. Modeling nongeminate recombination in p3ht:PCBM solar cells. 115(19):9806–9813.

- [27] Carsten Deibel, Alexander Wagenpfahl, and Vladimir Dyakonov. Influence of charge carrier mobility on the performance of organic solar cells. *physica status solidi (RRL)–Rapid Research Letters*, 2(4):175–177, 2008.
- [28] GAH Wetzelaer, M Kuik, M Lenes, and PWM Blom. Origin of the dark-current ideality factor in polymer: fullerene bulk heterojunction solar cells. *Applied physics letters*, 99(15):153506, 2011.